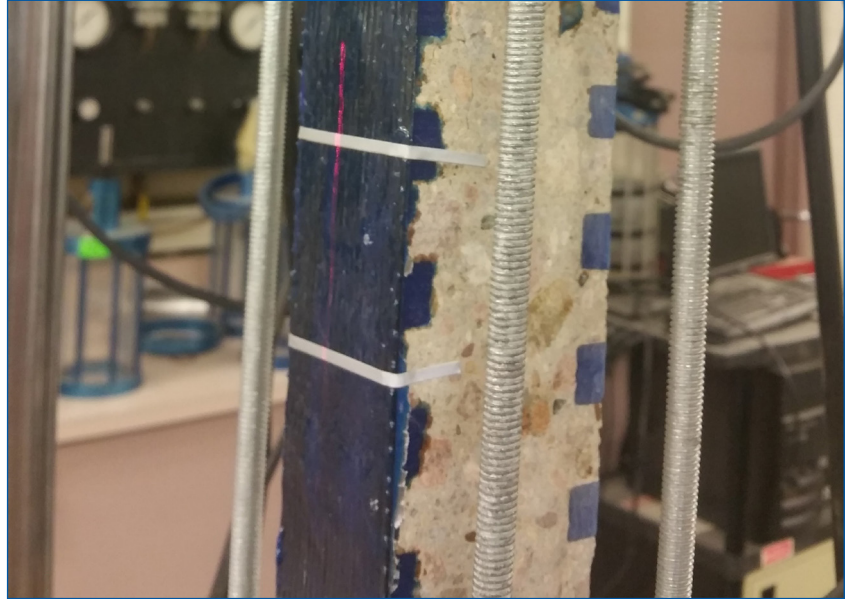


MOUNTAIN-PLAINS CONSORTIUM

MPC 19-402 | Y. J. Kim

Composite-Based
Rehabilitation of
Constructed Bridge Girders
with Grooved Geometrics



A University Transportation Center sponsored by the U.S. Department of Transportation serving the Mountain-Plains Region. Consortium members:

Colorado State University
North Dakota State University
South Dakota State University

University of Colorado Denver
University of Denver
University of Utah

Utah State University
University of Wyoming

Technical Report Documentation Page

1. Report No. MPC-554		2. Government Accession No.		3. Recipient's Catalog No.	
4. Title and Subtitle Composite-Based Rehabilitation of Constructed Bridge Girders with Grooved Geometrics				5. Report Date October 2019	
				6. Performing Organization Code	
7. Author(s) Yail Jimmy Kim, PhD				8. Performing Organization Report No. MPC 19-402	
9. Performing Organization Name and Address University of Colorado Denver 1200 Larimer Street Denver, CO 80217				10. Work Unit No. (TRAIS)	
				11. Contract or Grant No.	
12. Sponsoring Agency Name and Address Mountain-Plains Consortium North Dakota State University PO Box 6050, Fargo, ND 58108				13. Type of Report and Period Covered Final Report 9/2017 – 9/2022	
				14. Sponsoring Agency Code	
15. Supplementary Notes Supported by a grant from the US DOT, University Transportation Centers Program					
16. Abstract This report presents a research program studying the grooved bonding schemes of composite sheets (carbon fiber reinforced polymer, CFRP) for rehabilitating concrete members. The first phase of the research presents the efficacy of functional periodicity on controlling the occurrence of interfacial failure in concrete members strengthened with CFRP sheets. The hypothesis tested is that periodically placed stress reducers preserve the integrity of the CFRP-concrete interface by interrupting the progression of mechanical damage. The groove and U-wrap near the loaded-end dissipate interfacial fracture energy and impede stress progression. The second phase of the research discusses the potential and feasibility of an alternative bonding method for strengthening reinforced concrete beams with CFRP sheets. Periodic grooves are cut along the tensile soffit of the beams, in the transverse direction, on which CFRP is bonded and filled with an epoxy adhesive to lessen interfacial stresses. The tested bonding schemes comprise three grooves in the vicinity of CFRP-termination and uniformly distributed grooves in the beam span. The behavior of these beams is investigated in comparison with that of unstrengthened and conventional CFRP-bonded beams with plain substrates.					
17. Key Word bonding, carbon fibers, composite materials, debonding, epoxides, feasibility analysis, fiber reinforced polymers, girder bridges, rehabilitation (maintenance), shear stress			18. Distribution Statement Public distribution		
19. Security Classif. (of this report) Unclassified		20. Security Classif. (of this page) Unclassified		21. No. of Pages 47	22. Price n/a

Composite-Based Rehabilitation of Constructed Bridge Girders with Grooved Geometrics

Yail Jimmy Kim, Ph.D., P.Eng., FACI
Department of Civil Engineering
University of Colorado Denver
Denver, Colorado

October 2019

Acknowledgments

The Principal Investigator gratefully acknowledges all individuals contributed to the present research report.

Disclaimer

The contents of this report reflect the work of the author, who is responsible for the facts and the accuracy of the information presented. This document is disseminated under the sponsorship of the Mountain-Plains Consortium in the interest of information exchange. The U.S. Government assumes no liability for the contents or use thereof.

NDSU does not discriminate in its programs and activities on the basis of age, color, gender expression/identity, genetic information, marital status, national origin, participation in lawful off-campus activity, physical or mental disability, pregnancy, public assistance status, race, religion, sex, sexual orientation, spousal relationship to current employee, or veteran status, as applicable. Direct inquiries to: Vice Provost, Title IX/ADA Coordinator, Old Main 201, 701-231-7708, ndsueoaa@ndsu.edu.

EXECUTIVE SUMMARY

This report presents a research program studying the grooved bonding schemes of composite sheets (carbon fiber reinforced polymer, CFRP) for rehabilitating concrete members.

The first phase of the research presents the efficacy of functional periodicity on controlling the occurrence of interfacial failure in concrete members strengthened with CFRP sheets. The hypothesis tested was that periodically placed stress reducers preserve the integrity of the CFRP-concrete interface by interrupting the progression of mechanical damage. To substantiate this novel debonding-control concept, an experimental program is conducted with three types of stress reducers: epoxy-filled grooves (PG), discrete U-wraps (PU), and silyl-modified polymer (SMP) strips (PS). The load-carrying capacity of the PG and PU specimens is enhanced over 60% relative to the capacity of plain-bond control specimens (COT). The periodic configurations of these specimens (the number of grooves and U-wraps) influence the degree of capacity increase and failure modes by distributing interfacial stresses. Although capacity of the PS specimens was similar to that of the control, the permanent elastic nature of SMP improves the energy dissipation of the interface, which indicates the potential of the SMP-epoxy hybrid bond for seismic strengthening in tandem with other debonding-control methods. The groove and U-wrap near the loaded-end dissipate interfacial fracture energy and impede stress progression. Statistical inference alongside a probability-based assessment corroborated that the individual debonding-control methods and their configurations affected performance of the CFRP-concrete interface.

The second phase of the research discusses the potential and feasibility of an alternative bonding method for strengthening reinforced concrete beams with CFRP sheets. Periodic grooves were cut along the tensile soffit of the beams, in the transverse direction, on which CFRP was bonded and filled with an epoxy adhesive to lessen interfacial stresses. The tested bonding schemes comprised three grooves in the vicinity of CFRP-termination (the CG3 series) and uniformly distributed grooves in the beam span (the CGD series). The behavior of these beams was investigated in comparison with that of unstrengthened and conventional CFRP-bonded beams with plain substrates. The grooved beams exhibited more than a 46% higher load-carrying capacity relative to their conventional counterparts, dependent on a distance from the CFRP-termination to the nearest groove. Despite the occurrence of CFRP-delamination in the CG3 beams, the epoxy-filled grooves impeded the propagation and therefore, improved the beams' failure loads. For the CGD beams, CFRP-delamination was not observed until the beams failed by shear cracking and concrete crushing. The pre-yield stiffness of the grooved beams was enhanced due to the constrained concrete deformation and controlled cracking in tension. The CGD beams showed a stable growth in CFRP strain compared with the CG3 beams that experienced an irregular stress interaction between the CFRP and substrate. According to analytical modeling, the presence of the grooves at the CFRP-termination decreases interfacial stresses by up to 78%. The energy release rate of the grooved interface was examined to account for the integrity and delamination mechanisms of the proposed bonding approach.

TABLE OF CONTENTS

PART I: Functional Periodicity for Debonding-Control of CFRP-Concrete Interface

1. INTRODUCTION	1
2. RESEARCH SIGNIFICANCE	2
3. TEST PROCEDURE	3
3.1 Materials	3
3.2 Specimens and CFRP-bonding Schemes	3
3.3 Test Setup and Instrumentation	4
4. EXPERIMENTAL RESULTS	5
4.1 Load-carrying Capacity	5
4.2 Failure Mode	7
4.3 Load-displacement Behavior	7
4.4 Interfacial Fracture Energy	8
4.5 Development of CFRP Strain	10
4.6 CFRP-strain Profile	11
5. STATISTICAL ASSESSMENT	14
5.1 Analysis of Variance	14
5.2 Inference with <i>t</i> -test	15
5.3 Evaluation of Error in Hypotheses	16
6. SUMMARY AND CONCLUSIONS	18
7. REFERENCES	19

PART II. Debonding-Mitigation of CFRP-Strengthened RC Beams with Grooved Bonding

8. INTRODUCTION	20
9. RESEARCH SIGNIFICANCE	21
10. EXPERIMENTAL PROGRAM	22
10.1 Materials	22
10.2 Beam Preparation	22
10.3 Strengthening Details	22
10.4 Test Setup	24

11. TEST RESULTS.....	25
11.1 Beam Capacity.....	25
11.2 Failure Mode.....	25
11.3 Flexural Behavior	27
11.4 Profile of CFRP Strain.....	29
11.5 Progression of Delamination and Cracking.....	30
12. MODELING OF STRESS TRANSFER	32
12.1 Local Response by Interfacial Shear	32
12.2 Global Response by Beam Bending	33
13. SUMMARY AND CONCLUSIONS.....	36
14. REFERENCES	38

LIST OF TABLES

[PART I]

Table 4.1	Test specimens	6
Table 5.1	Analysis of Variance for debonding-control methods at variable significance levels	14
Table 5.2	Probability of correctly rejecting false H_0 hypothesis	17

[PART II]

Table 10.1	Test matrix.....	23
------------	------------------	----

LIST OF FIGURES

[PART I]

Figure 3.1	Test specimens	4
Figure 4.1	Load-carrying capacity	5
Figure 4.2	Failure mode	8
Figure 4.3	Load-displacement	9
Figure 4.4	Interfacial fracture energy	10
Figure 4.5	Load-strain behavior	11
Figure 4.6	Profile of CFRP strains	12
Figure 4.7	Comparison of CFRP strain	13
Figure 5.1	t -test results for configuration of debonding-control methods	15
Figure 5.2	Operating characteristic curve	16

[PART II]

Figure 10.1	Beam details	23
Figure 10.2	Test setup and instrumentation	24
Figure 11.1	Load-carrying capacity	25
Figure 11.2	Failure modes	26
Figure 11.3	Load-displacement of beams	27
Figure 11.4	Load-strain behavior at midspan	28
Figure 11.5	CFRP strain profile	30
Figure 11.6	Crack development	31
Figure 12.1	Shear stress profile at a load of 5 kN	34
Figure 12.2	Development of steel and CFRP strains due to bending at near-failure of beams	36
Figure 12.3	Assessment of integrity in CFRP-concrete interface	36

PART I: Functional Periodicity for Debonding-Control of CFRP-Concrete Interface

1. INTRODUCTION

Carbon fiber reinforced polymer (CFRP) composites have been used for decades to enhance the performance of structurally deficient concrete members. When CFRP sheets are bonded to the tensile side of a beam, internal forces are rearranged to achieve equilibrium that increases the flexural capacity. From a design standpoint, the bonded CFRP should not fail by debonding until the concrete is crushed (compression-control). Typical debonding failure modes in a reinforced concrete beam strengthened with CFRP involve: i) *peel-off* at the termination of the CFRP and ii) *intermediate-crack-induced debonding* (IC-debonding) along the CFRP-concrete interface. To maintain the load-carrying capacity of a strengthened beam, appropriate stress transfer is indispensable between the concrete substrate and CFRP. Excessive mechanical loading causes premature failure of the interface, which is of primary interest in practice. While CFRP sheets are epoxy-bonded without explicit debonding-control on many occasions, wide U-wraps are often placed to alleviate the possibility of peel-off failure (Baky et al. 2007). As far as IC-debonding is concerned, published design guidelines (for example, ACI 440.2R-17, ACI 2017) recommend that the effective strain of CFRP remains below a certain limit to preserve integrity of the interface. Although this concept is broadly employed, an intrinsic drawback exists because the strain limit has been empirically determined. To overcome such limitations, alternative approaches (explicit debonding-control) were proposed by several researchers. Mostofinejad and Mahmoudabadi (2010) examined effects of substrate-slitting on the failure of CFRP-bonded concrete prisms. Specimens with multiple slits in the transverse and longitudinal directions showed a capacity increase of 15% relative to those with a plain substrate. The failure of the substrate-slit specimens was attributed to CFRP-rupture, rather than debonding, which means the full tensile strength of the CFRP was used. Kim et al. (2014) studied the potential of CFRP spike anchors inserted into predrilled holes in reinforced concrete T-beams strengthened with CFRP sheets. Of interest was the usable strain of the externally-bonded CFRP up to failure. Owing to mechanical action of the spike anchors, detachment of the CFRP was not noticed even after the local failure of the adhesive (debonding). Eftkhar and Ya'ghubi (2016) drilled multiple holes into the substrate of concrete prisms on which CFRP sheets were bonded with an epoxy to distribute contact stresses. This postponed the occurrence of debonding failure. The proposed method increased the capacity and ductility of test specimens; however, CFRP-debonding was still observed. Lee and Lopez (2016) studied the effectiveness of U-wraps on preventing the debonding failure of CFRP sheets longitudinally bonded to reinforced concrete beams. The performance of U-wraps was satisfactory in terms of debonding-control and an increase in the load-carrying capacity of the strengthened beams. The geometric properties of U-wraps and corresponding frictional characteristics on a concrete substrate were noted to be important. Wu et al. (2016) conducted experiments using a mechanical anchor system composed of steel bolts and strips to avoid CFRP-debonding. An analytical model was developed and compared against test data to understand the load-bearing mechanisms of the anchor system (adhesion, dowel action, and friction) bonded to a concrete substrate.

Despite the endeavors mentioned here, further research is needed to develop effective debonding-control approaches. In this study, a new concept was proposed by decoupling the development of interfacial stress from debonding failure. The concept is accomplished through periodic placement of stress reducers along a bondline, which repeatedly discontinues the progression of the interfacial stress: i) multiple grooves filled with an epoxy, ii) discrete narrow U-wraps, and iii) silyl-modified polymer (SMP) strips. An experimental program was conducted with a hypothesis that these functional periodicities relieve interfacial stresses and, as a consequence, the load-carrying capacity of the interface is enhanced. Test results are statistically characterized and probabilistically assessed.

2. RESEARCH SIGNIFICANCE

The integrity of CFRP-concrete interface is salient, and its failure — in whole or part — should be precluded. Premature debonding hinders the expected functionality of a CFRP-strengthening system and the use of CFRP's high tensile strength. Two approaches are available to address debonding problems: i) development of a CFRP strain is controlled below a prescribed limit (implicit) and ii) external attributes are utilized to physically restrain the deformation of the interface (explicit). The implicit method prevails in design guidelines, albeit insufficient, owing to the eidetic and straightforward execution. This research experimentally substantiates the feasibility of an explicit debonding-control concept based on functional periodicity.

3. TEST PROCEDURE

An experimental program dedicated to exploring effective debonding-control methods for CFRP-strengthened concrete members is described, including the details of materials, various bonding schemes, and a test method.

3.1 Materials

The specified concrete strength in compression was 20 MPa (2,900 psi) and cylinder tests at 28 days showed an average strength of 19 MPa (2,800 psi). CFRP sheets are composed of unidirectional carbon fibers and an epoxy resin, which led to a nominal tensile strength of 3,800 MPa (550 ksi), a modulus of 227 GPa (32,900 ksi), and a rupture strain of 1.67% in conjunction with an equivalent fiber thickness of 0.165 mm (0.006 in.). The epoxy resin was also used as a bonding agent between the concrete and CFRP with the following mechanical properties: tensile strength = 55 MPa (7,980 psi), elastic modulus = 2.6 GPa (377 ksi), Poisson's ratio = 0.4, and failure strain = 2.9%. Another adhesive type employed was silyl-modified polymer (SMP) that is a solvent-free material. The SMP adhesive demonstrates permanent elastic behavior combining the benefits of silicon and polyurethane; accordingly, it can absorb significant strain energy prior to failure. The nominal properties of SMP involve a tensile strength of 2.6 MPa (375 psi) and a modulus of 3.3 MPa (475 psi) at a rupture strain of 250%.

3.2 Specimens and CFRP-bonding Schemes

Concrete blocks were prepared with dimensions of 50 mm (2 in.) by 100 mm (4 in.) by 300 mm (12 in.). After moisture-curing for 28 days in a humidity room (99% humidity at 23°C (73°F), on average), the blocks were removed, water-washed, dried, and cleaned with an airbrush. A single layer of CFRP sheet (50 mm (2 in.) wide by 430 mm (17 in.) long) was bonded to each block using the epoxy adhesive (that is, control specimens with plain CFRP-bonding, designated to be COT) together with the following debonding-control methods, as illustrated in Figure 3.1:

- PG: the concrete blocks were cut to create grooves (20 mm (0.8 in.) wide by 15 mm (0.6 in.) deep) using a diamond saw. The grooves were then filled with the epoxy to mitigate development of interfacial stresses when the CFRP sheet was loaded (the CFRP was bonded along the concrete substrate immediately after filling the grooves to achieve a monolithic interface).
- PU: the epoxy was uniformly applied along the plain concrete substrate on which the CFRP sheet was impregnated and bonded. Precut CFRP U-wraps (20 mm (0.8 in.) wide by 210 mm (8.3 in.) long) were then epoxy-bonded.
- PS: the SMP and epoxy adhesives were alternately applied along the concrete substrate (hybrid bonding), followed by the impregnation of the CFRP sheet.

The initial position of the debonding mitigation elements (grooves, U-wraps, and SMP strips) near the loaded-end addressed the occurrence of IC-debonding, as suggested by ACI 440.2R-17 (ACI 2017). The specimens were cured for a minimum of seven days in compliance with the manufacturer's guidelines, except for those bonded with SMP that required a curing time of two weeks. It should be noted that a 25 mm (1 in.) unbonded zone was included in all cases (Figure 3.1) to avoid stress concentrations when mechanically loaded. Each test category was replicated five times.

3.3 Test Setup and Instrumentation

The cured specimen was placed in a custom-made fixture mounted to a universal testing machine. The jacking-end of the CFRP sheet was epoxy-impregnated for gripping resistance, thereby evading premature slippage (this process was performed after the CFRP-concrete interface was fully cured). A non-contacting laser extensometer was employed with reflection tapes to measure displacement of the CFRP immediately beyond the unbonded region (Figure 3.1), where a maximum interfacial response takes place. Strain gages were bonded along the CFRP sheet at a center-to-center spacing of 25 mm (1 in.). The specimen was monotonically tensioned at a rate of 0.3 mm (0.012 in.) per min. until failure, and the behavior was recorded by a computerized data acquisition system.

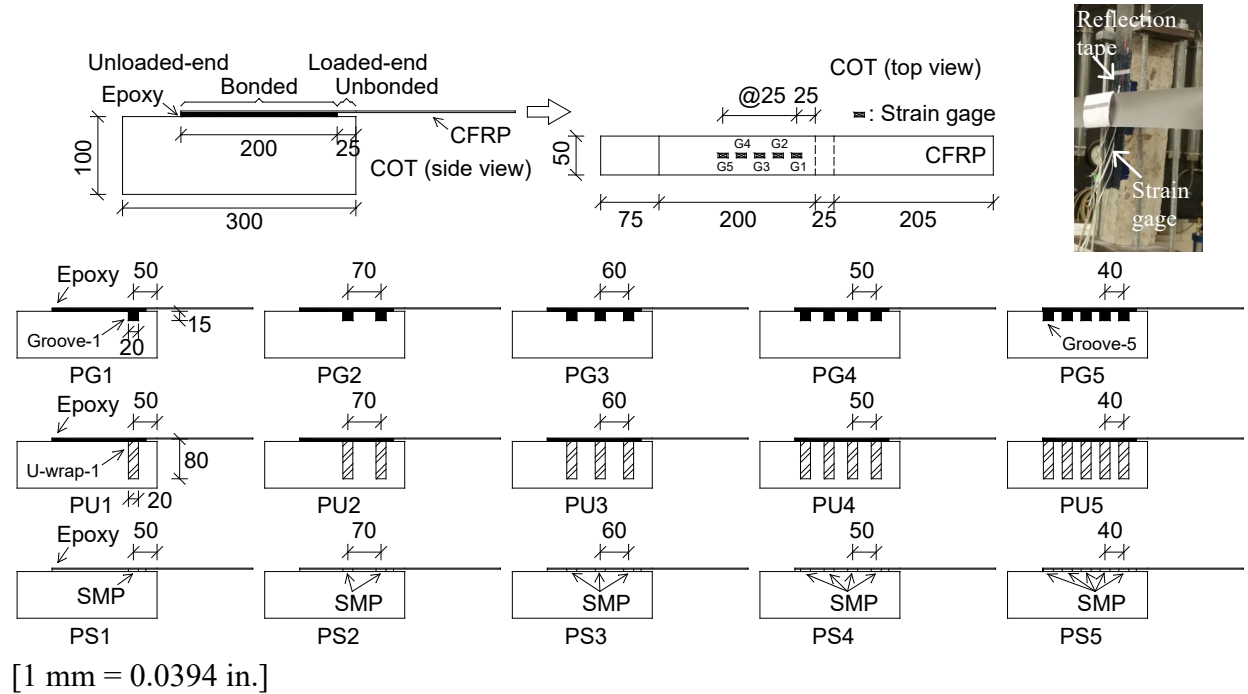


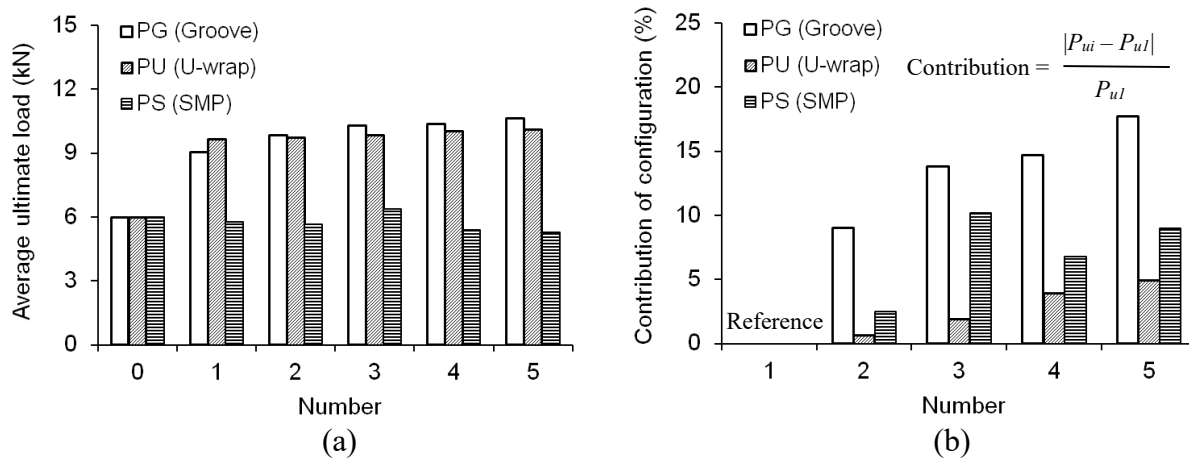
Figure 3.1 Test specimens (units in mm)

4. EXPERIMENTAL RESULTS

The succeeding sections provide test observations and corresponding discussions. Emphasis was placed on the integrity of CFRP-concrete interface, failure characteristics, fracture energy, and strain development.

4.1 Load-carrying Capacity

The capacity of the CFRP-concrete interface is enumerated in Table 4.1 and summarized in Figure 4.1(a). The average ultimate loads of the PG specimens with one- and two-grooves (PG1 and PG2) were 50.7% and 64.3% higher than the plain control specimens (COT), respectively. This increasing trend slowed down when more grooves were added (71.5%, 72.8%, and 77.5% for the three-, four- and five-groove specimens, respectively). The first epoxy-filled groove near the loaded-end (Groove-1) mitigated development of a stress singularity. As such, shear stresses along the interface were limitedly transferred to the subsequent grooves. Specimens with U-wraps (the PU series) showed load-carrying capacities similar to their PG counterparts at an average absolute difference of 4.5%. Due to the low strength of SMP, capacities of the specimens with hybrid bonding (the PS series) were lower than those of the PG and PU categories. It is worth noting that use of the SMP adhesive was intended to examine its energy absorption capability associated with the permanent elastic nature, thus controlling the interfacial stresses, rather than to increase the load-carrying capacity of the specimens. Figure 4.1(b) evaluates the contribution of periodic configurations (the number of grooves, U-wraps, and SMP strips) to the capacity of CFRP-concrete interface. Notwithstanding the likeness of the capacity variations in the PG and PU specimens (Figure 4.1(a)), the groove numbers had a more pronounced impact on the capacity increase than the U-wrap numbers. For example, capacities with five grooves (PG5) and five U-wraps (PU5) rose by 17.7% and 4.9% compared with capacity with the reference number (PG1 and PU1), respectively (Figure 4.1(b)). The contribution of SMP-strip numbers was also notable; however, inconsistent responses were observed owing to the erratic failure of the permanently-elastic adhesive that affected the stress transfer from an epoxy-bonded zone to another (further discussion is available in the following sections).



[1 kN = 0.225 kips]

Figure 4.1 Load-carrying capacity: (a) comparison among debonding-control methods; (b) contribution of periodic configurations (P_{ui} = capacity of specimen with number i ; P_{u1} = capacity of specimen with number one)

Table 4.1 Test specimens

ID	Debonding control		Ultimate load (kN)		ID	Debonding control		Ultimate load (kN)	
	Method	No.	Each	Ave		Method	No.	Each	Ave
COT-1	None	0	6.65	5.99	PU3-1	U-wrap	3	8.73	9.83
COT-2	None	0	6.58		PU3-2	U-wrap	3	9.76	
COT-3	None	0	6.18		PU3-3	U-wrap	3	9.16	
COT-4	None	0	5.20		PU3-4	U-wrap	3	10.72	
COT-5	None	0	5.34		PU3-5	U-wrap	3	10.79	
PG1-1	Groove	1	9.18	9.03	PU4-1	U-wrap	4	9.94	10.03
PG1-2	Groove	1	7.76		PU4-2	U-wrap	4	10.26	
PG1-3	Groove	1	9.25		PU4-3	U-wrap	4	8.33	
PG1-4	Groove	1	10.51		PU4-4	U-wrap	4	11.30	
PG1-5	Groove	1	8.44		PU4-5	U-wrap	4	10.30	
PG2-1	Groove	2	9.49	9.84	PU5-1	U-wrap	5	10.67	10.12
PG2-2	Groove	2	9.79		PU5-2	U-wrap	5	8.98	
PG2-3	Groove	2	10.87		PU5-3	U-wrap	5	9.20	
PG2-4	Groove	2	8.25		PU5-4	U-wrap	5	11.22	
PG2-5	Groove	2	10.79		PU5-5	U-wrap	5	10.53	
PG3-1	Groove	3	9.74	10.27	PS1-1	SMP	1	6.23	5.79
PG3-2	Groove	3	11.11		PS1-2	SMP	1	4.94	
PG3-3	Groove	3	8.77		PS1-3	SMP	1	5.80	
PG3-4	Groove	3	11.43		PS1-4	SMP	1	5.83	
PG3-5	Groove	3	10.30		PS1-5	SMP	1	6.13	
PG4-1	Groove	4	11.27	10.35	PS2-1	SMP	2	5.99	5.64
PG4-2	Groove	4	11.07		PS2-2	SMP	2	5.55	
PG4-3	Groove	4	10.77		PS2-3	SMP	2	5.87	
PG4-4	Groove	4	9.55		PS2-4	SMP	2	5.76	
PG4-5	Groove	4	9.10		PS2-5	SMP	2	5.05	
PG5-1	Groove	5	12.84	10.63	PS3-1	SMP	3	6.23	6.38
PG5-2	Groove	5	10.22		PS3-2	SMP	3	6.99	
PG5-3	Groove	5	11.52		PS3-3	SMP	3	7.03	
PG5-4	Groove	5	10.20		PS3-4	SMP	3	6.58	
PG5-5	Groove	5	8.37		PS3-5	SMP	3	5.06	
PU1-1	U-wrap	1	9.97	9.65	PS4-1	SMP	4	4.90	5.40
PU1-2	U-wrap	1	8.60		PS4-2	SMP	4	5.46	
PU1-3	U-wrap	1	8.76		PS4-3	SMP	4	6.26	
PU1-4	U-wrap	1	11.67		PS4-4	SMP	4	5.68	
PU1-5	U-wrap	1	9.24		PS4-5	SMP	4	4.68	
PU2-1	U-wrap	2	8.40	9.71	PS5-1	SMP	5	5.16	5.27
PU2-2	U-wrap	2	10.28		PS5-2	SMP	5	4.47	
PU2-3	U-wrap	2	9.10		PS5-3	SMP	5	6.02	
PU2-4	U-wrap	2	10.75		PS5-4	SMP	5	5.96	
PU2-5	U-wrap	2	10.03		PS5-5	SMP	5	4.74	

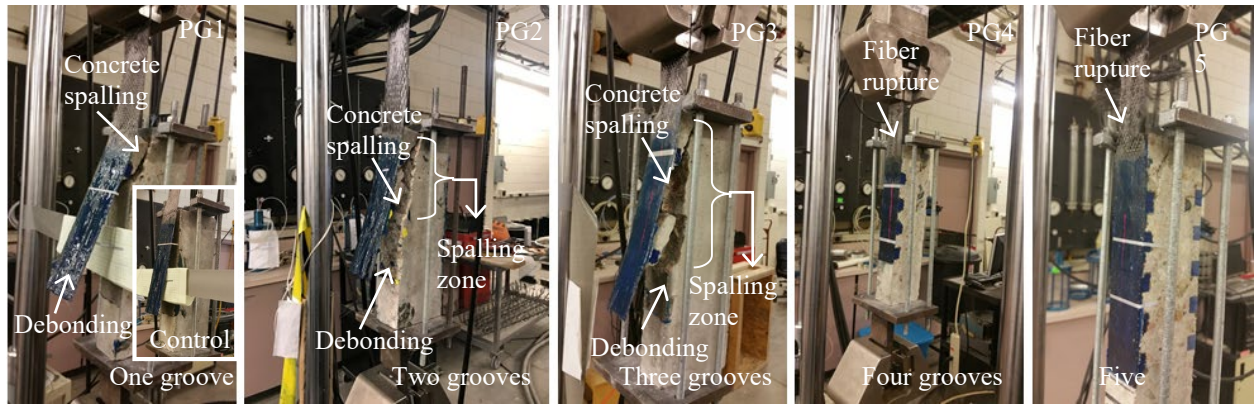
No.: number of functional periodicity

4.2 Failure Mode

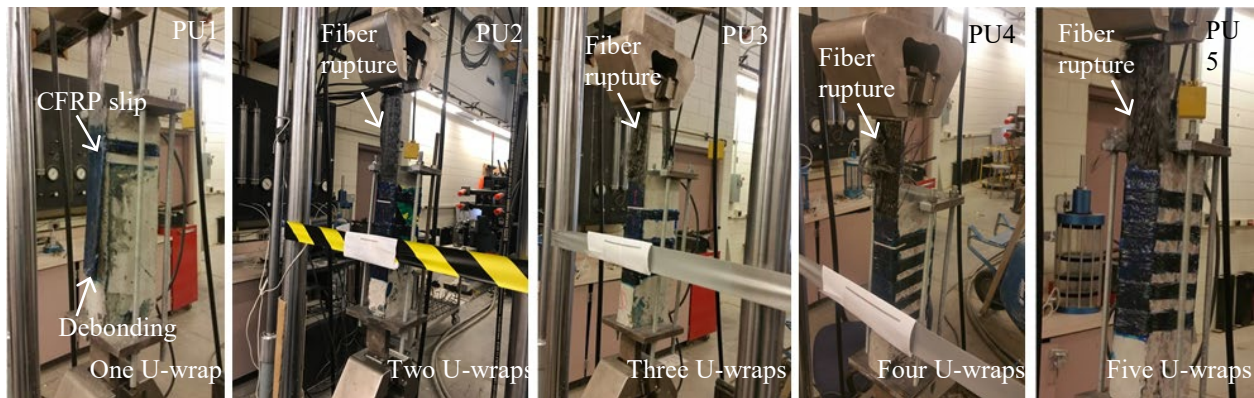
Various failure modes were observed for the specimens depending on strengthening schemes, as summarized in Figure 4.2. Dissimilar to the control case (COT) exhibiting typical CFRP-debonding (Figure 4.2(a), inset), the PG1 specimen (one groove) showed concrete spalling near the loaded-end. This response is attributable to the presence of the groove that preserved integrity of the CFRP-concrete interface (that is, the stress applied to the CFRP was transferred to the concrete substrate through the epoxy-filled groove). The specimens with two and three grooves (PG2 and PG3, respectively) supported the foregoing stress-transfer mechanism, incorporating widened spalling regions. As the number of grooves further increased (four and five grooves), the failure mode shifted from debonding to fiber-rupture. Therefore, the proposed groove-bonding scheme can preclude the incidence of CFRP-debonding, as long as the interfacial stress is sufficiently transferred to the concrete substrate. Figure 4.2(b) reveals the failure of the U-wrapped specimens. With the use of a single U-wrap (PU1), debonding occurred with the slip of the CFRP through the U-wrap — the resistance of the U-wrap was not enough to mitigate interfacial stress. Increasing the number of U-wraps controlled debonding and failure of the specimens took place outside the CFRP-concrete interface (that is, fiber-rupture). This finding demonstrates that use of discrete U-wraps is an effective means to alleviate development of interfacial stresses, and such a bonding scheme is recommendable to address the IC-debonding of a CFRP-strengthened beam (instead of impractical continuous U-wraps along the beam span). Irrespective of SMP-strip numbers, all PS specimens failed by debonding, as shown in Figure 4.2(c). The SMP-based hybrid bonding, therefore, should be used with other methods such as the PG and PU series, so the SMP's unique feature on energy dissipation (to be elaborated) can provide a synergetic debonding-control approach.

4.3 Load-displacement Behavior

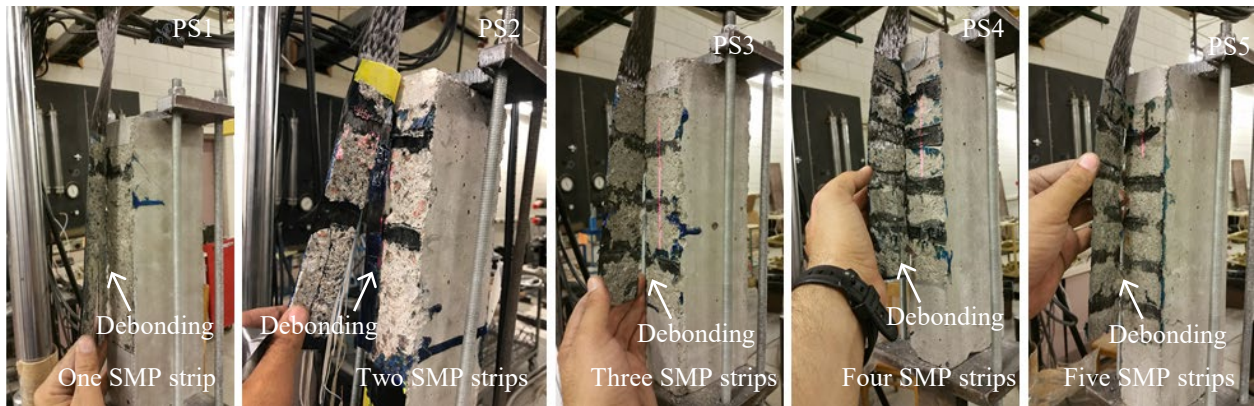
Figure 4.3 shows the load-displacement behavior of selected specimens. The displacement of the case with plain-bonding (COT) linearly increased until abrupt failure occurred at a load of 6.2 kN (1.4 kips). Behavior of the grooved specimens (PG) was essentially linear as in the case of the control (Figure 4.3(a)). Local fluctuation was noticed in all except the one-grooved specimen (PG1), which was ascribed to the fact that multiple grooves periodically interrupted the transfer of shear stresses along the bond line from the loaded-end to the other end. Specimens with U-wraps (PU) revealed linear responses without local fluctuation noted in the PG specimens (Figure 4.3(b)), meaning that interfacial stresses in the PU categories were effectively distributed by the U-wraps. Unlike these two categories, the SMP-epoxy hybrid bond specimens (PS) exhibited stepwise responses (Figure 4.3(c)). This observation can be explained by the low modulus of SMP that expedited transfer of the interfacial stresses between the discrete epoxy-bonded regions accompanied by the so-called *stop-and-go* load increment (Figure 4.3(c), inset). The representative behavior of specimens with the maximum number of the grooves, U-wraps, and SMP strips is compared in Figure 4.3(d). The load-carrying capacity of PG5 was the highest with the largest displacement at failure. Contrary to the other specimens, PU5 upheld stiffness without a reduction since the U-wraps had integrated with the longitudinal CFRP, as explained above. The displacement of PS5 was larger than those of COT and PU5, indicating the potential of the proposed hybrid bonding scheme for seismic strengthening application that requires significant energy consumption and dissipation.



(a)

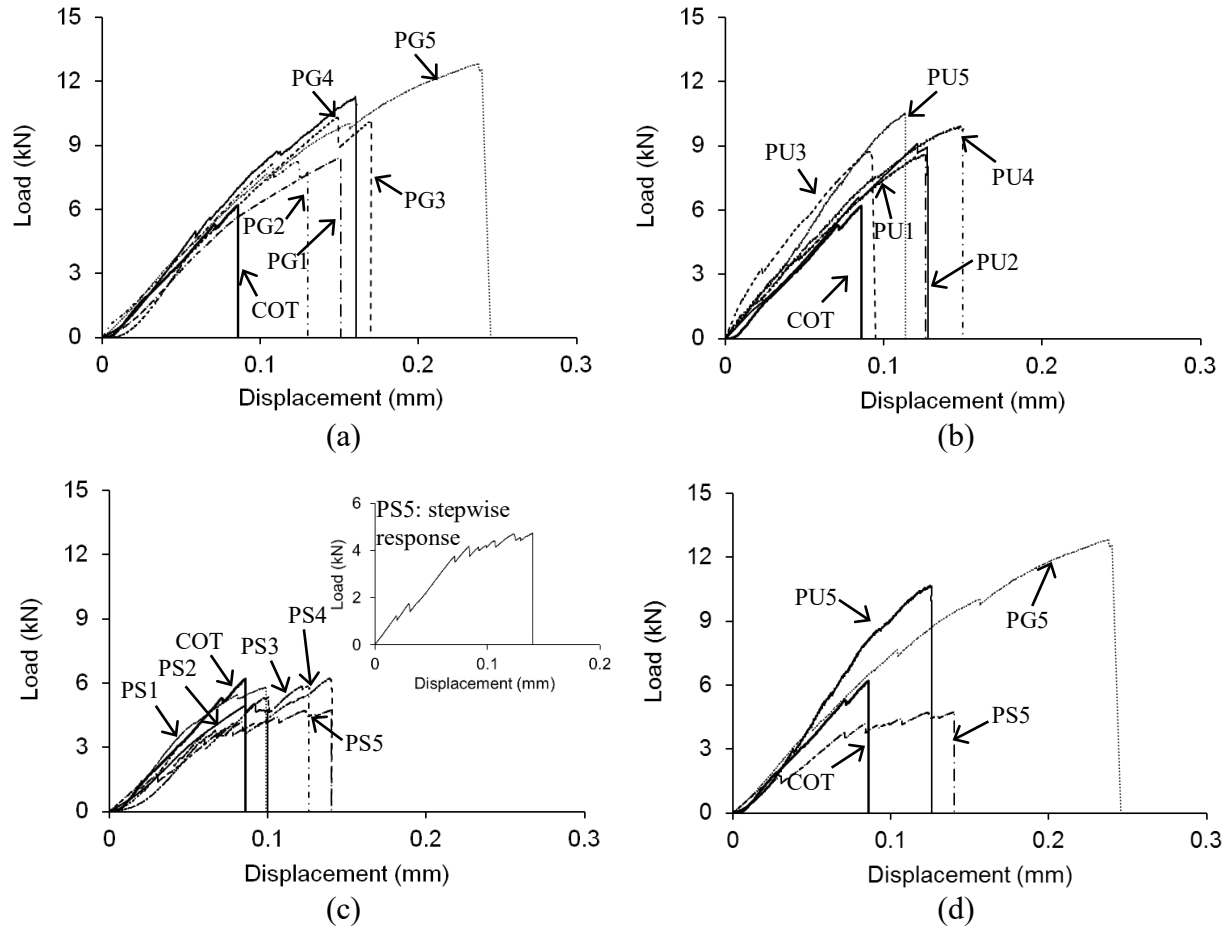


(b)



(c)

Figure 4.2 Failure mode: (a) control (COT); (b) groove (PG); (c) U-wrap (PU); (d) SMP (PS)



[1 kN = 0.225 kips; 1 mm = 0.0394 in.]

Figure 4.3 Load-displacement: (a) PG (groove); (b) PU (U-wrap); (c) PS (SMP); (d) comparison

4.4 Interfacial Fracture Energy

Figure 4.4 shows the interfacial fracture energy (G) associated with various bonding schemes up to the maximum load of each specimen (P_u), which was acquired by Eq. I.1 alongside a numerical integration technique (the trapezoidal rule)

$$G = \sum_{i=1}^n \tau_i \delta_i \quad (I.1)$$

where τ_i is the average interfacial shear stress at the i^{th} load state (a load P_i divided by the CFRP-bonded area of 10,000 mm² (15.5 in.²), as shown in Figure 3.1) and δ_i is the displacement coupled with P_i in the load-displacement curve of the specimen with n segments. Average interfacial fracture energy of the PG series was 451% higher than the energy of the control (number zero in the abscissa of Figure 4.4), including the 438% increase of the one-grooved case (PG1). The PU series revealed higher interfacial fracture energies relative to the control (an average increase of 228%), whereas the level of improvement was lower than that of the PG series. This fact is attributable to increased displacement of the PG specimens at failure because the epoxy-filled grooves retarded CFRP-debonding by reducing interfacial

stresses, as noted previously. From a theoretical point of view (Smith and Teng 2001), the interfacial stress comprises normal and shear components along the CFRP bond line, both are a function of the adhesive thickness (the epoxy-filled grooves vs. plain epoxy thickness in the present case). While the PS category's fracture energy was lower than the others, the former demonstrated a 92% higher energy dissipation, on average, compared with the control (number zero in Figure 4.4).

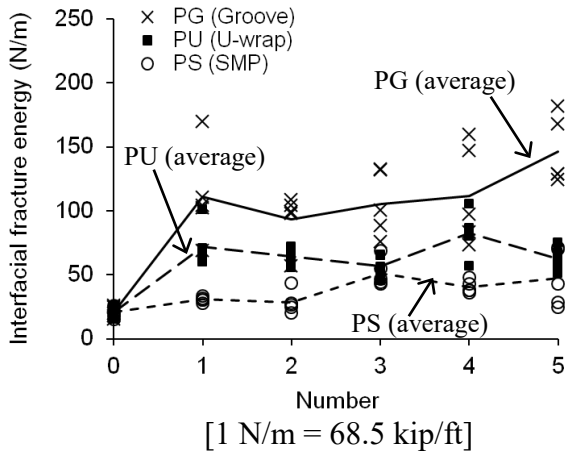
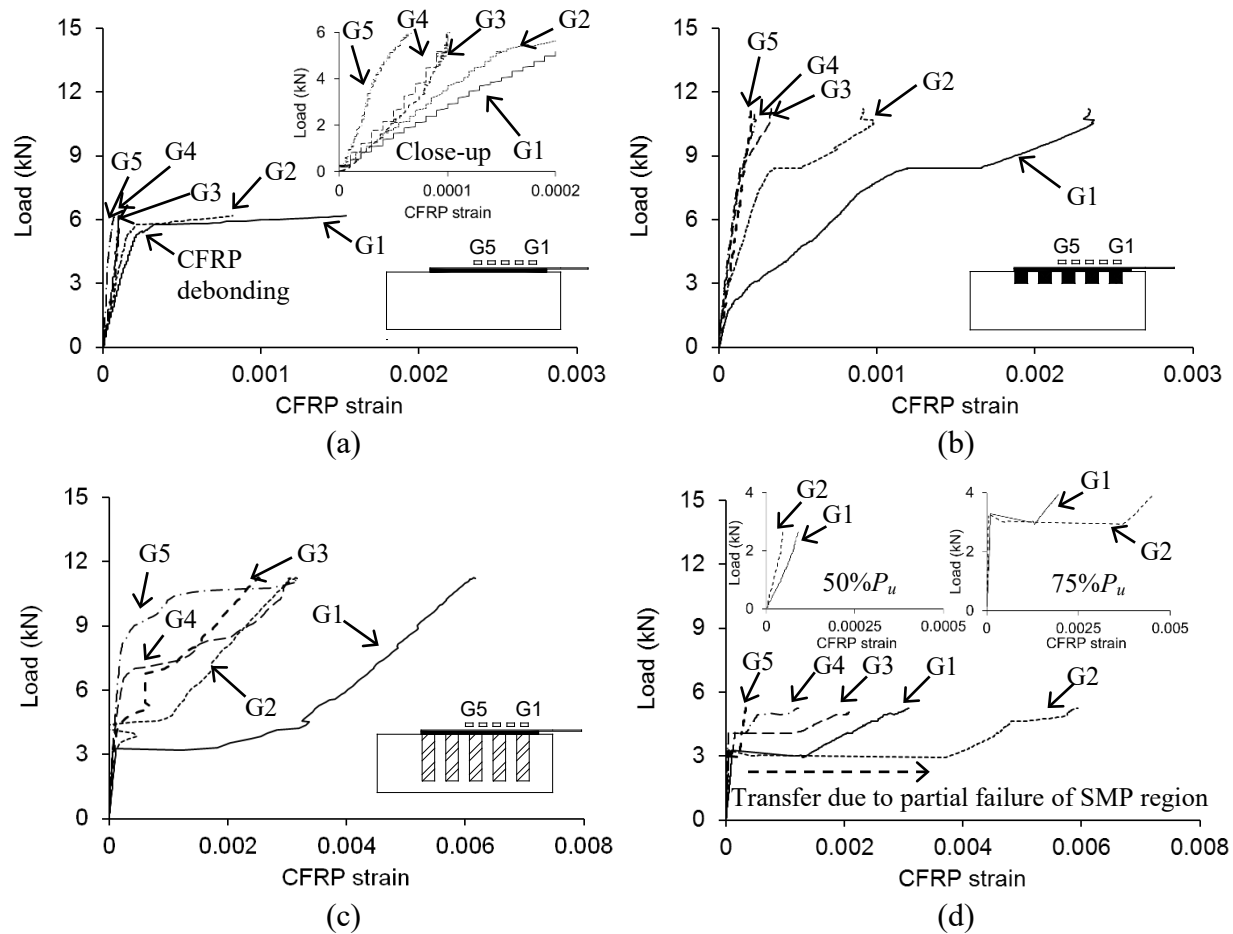


Figure 4.4 Interfacial fracture energy

4.5 Development of CFRP Strain

The load-CFRP strain behavior of the individual categories is provided in Figure 4.5. Slopes of the strain development were preserved in the control case until CFRP-debonding occurred (Figure 4.3(a)). The strain magnitudes were influenced by distance from the unbonded zone where a geometric discontinuity existed. In other words, the closer the location is to a stress singularity, the higher its strain becomes (Figure 4.5(a), inset). For the specimen with five grooves (PG5), the sequential strain transfer along the CFRP-bond line was more apparent than that of the control, as shown in Figure 4.5(b). The early deviation of the response slope in strain gage G1 is ascribed to the shear deformation of the epoxy that filled Groove-1, close to the unbonded zone. Given that the strain development of gage G2 was consistent up to a load of 8.3 kN (1.9 kips), Groove-1 appears to dissipate a significant amount of energy that impeded the transfer of the interfacial stress to the next gage. This trend was also valid for subsequent strain readings in gages G3 to G5, which implies the effectiveness of the grooved bonding scheme in terms of upholding interfacial integrity through the stable stress transfer mechanism. The strain development of the U-wrapped specimen (PG5) was in conformance with that of the previous cases (that is, sequential strain increases), except for the irregular strain readings (Figure 4.5(c)). For instance, gage G1 showed a noticeable strain of $3,320 \times 10^{-6}$ at a load of 4.4 kN (1 kip) owing to the deformation of the U-wrap that was bonded in the transverse direction (unlike the longitudinal CFRP, the fiber orientation of the U-wrap was perpendicular to the loading direction; as a result, the carbon fibers embedded in the U-wrap could not carry the load). Figure 4.5(d) reveals the CFRP strain of the SMP-bonded specimen (PS5). Although the sequential strain propensity was generally maintained, partial failure of the SMP strip near the unbonded zone affected the readings of gage G1 and the interfacial strains transferred to the adjacent strips were recorded by gage G2. The insets of Figure 4.5(d) clarify the transition of the strain development in gages G1 and G2.



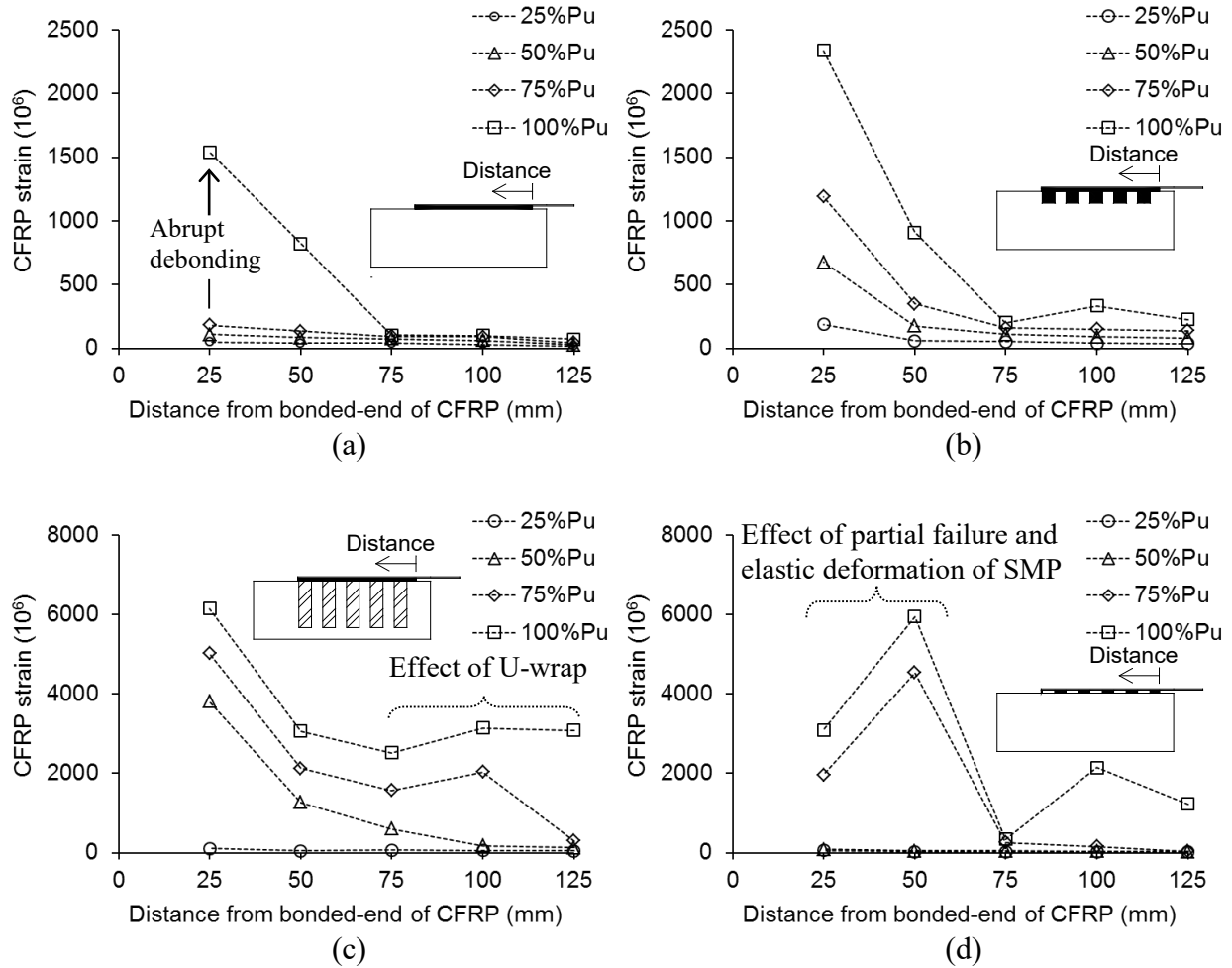
[1 kN = 0.225 kips]

Figure 4.5 Load-strain behavior: (a) control (COT); (b) grooved specimen (PG5); (c) U-wrapped specimen (PU5); (d) SMP-epoxy hybrid bond (PS5)

4.6 CFRP-strain Profile

Figure 4.6 exhibits the profile of CFRP strains along the interface. The strain values of the control specimen were low up to a load level of $75\%P_u$ (the maximum strain recorded was 1.1% of the CFRP's rupture strain), as shown in Figure 4.6(a). By contrast, an abrupt strain increase was noticed on the brink of CFRP-debonding failure at $100\%P_u$ with a maximum strain of $1,540 \times 10^{-6}$ (9.2% of the rupture strain). Strain development of the specimen with grooves (PG5) was steady until the fiber-rupture took place (Figure 4.6(b)). The maximum usable CFRP strain of the PG5 specimen was 52% higher than that of the control, which again confirms efficacy of the proposed bonding scheme with multiple grooves. The insignificant strains of the control and the grooved specimens beyond 75 mm (3 in.) from the bonded-end (a maximum of 1.1% and 2.0% of the rupture strain, respectively) show that the interfacial stresses near the loaded-end were not fully transferred to the other side. On the other hand, because of the transverse fiber direction in the U-wraps explained earlier, remarkable strain increases were observed in the U-wrapped specimen (PU5) even at a service load level of $50\%P_u$ (Figure 4.6(c)). Despite the fact that strain propagation toward the unloaded-end was apparent in the U-wrapped specimen, complete debonding of the longitudinal CFRP was precluded by the presence of multiple U-wraps (Figure 4.2(b)). Furthermore, the pattern of strain increase in the CFRP-bonded region between 25 mm (1 in.) and 75 mm (3 in.) was

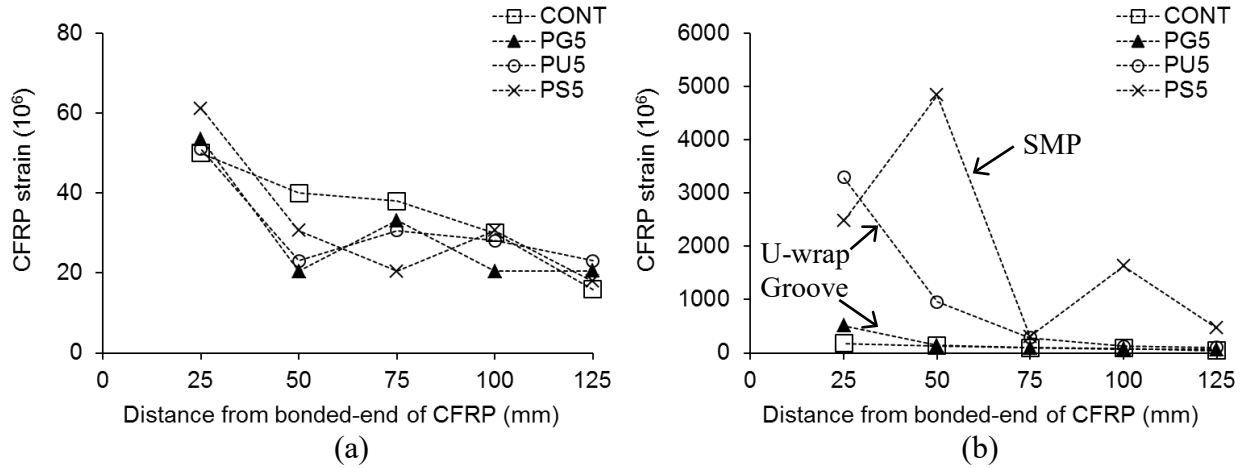
constant from 50% P_u to 100% P_u and the strains between 75 mm (3 in.) and 125 mm (5 in.) were below $3,138 \times 10^{-6}$ (18.8% of the rupture strain). The strain profile of the SMP-bonded specimen (PS5) was different from that of the other cases, as shown in Figure 4.6(d). Due to the partial interface failure with elastic deformation of the SMP-bonded zone, fluctuating strain profiles were recorded. The strain of $2,141 \times 10^{-6}$ belonging to gage G4 bonded on an SMP zone at 100% P_u indicates that the interfacial stresses were transferred through the preceding epoxy-bonded zone.



[1 mm = 0.0394 in.]

Figure 4.6 Profile of CFRP strains: (a) control (COT); (b) grooved specimen (PG5); (c) U-wrapped specimen (PU5); (d) SMP-epoxy hybrid bond (PS5)

A comprehensive comparison among the bonding schemes is made in Figure 4.7 at $25\%P_u$ and $75\%P_u$ of the control specimen ($P_u = \text{control capacity}$), which respectively represents interfacial strains below and above the typical service load level of $50\%P_u$. The CFRP strains of the specimens with the grooves, U-wraps, and SMP strips were generally lower than those of the control specimen at $25\%P_u$ (Figure 4.7(a)). Such strain trends, however, changed as a load level increased to $75\%P_u$ (Figure 4.7(b)), particularly for the U-wrapped and SMP-bonded cases due to the fiber-orientation and the partial SMP failure, respectively, that were detailed earlier.



[1 mm = 0.0394 in.]

Figure 4.7 Comparison of CFRP strain: (a) at 25% of control capacity (COT); (b) at 75% of control capacity (COT)

5. STATISTICAL ASSESSMENT

To characterize the efficacy of various debonding-control methods, statistical approaches are exploited. The background of the individual approaches and assessment results are elaborated in this section.

5.1 Analysis of Variance

The aforementioned debonding-control methods were evaluated by the Analysis of Variance (ANOVA) at variable significance levels from $\alpha = 0.05$ to 0.25 . The following hypotheses were tested: $H_0: \bar{x} = \mu$ and $H_a: \bar{x} \neq \mu$, where \bar{x} is the mean response of the respective debonding-control method (one of the PG, PU, and PS categories) and μ is the mean response of the control specimens (COT). If an F distribution value is in the critical domain at a certain significance level ($F \geq F_{critical}$), the hypothesis H_0 is rejected. Table 5.1 lists F distribution values obtained from the sum of squares, degrees of freedom, and mean square (Montgomery 2013) for the debonding-control methods and their periodic configurations (the number of the grooves, U-wraps, and SMP strips). The calculated F values specify that the difference among the debonding-control methods (*Methods* in Table 5.1) was statistically significant at all significance levels ($F = 156.67 > F_{0.05} = 3.15 > F_{0.10} = 2.39 > F_{0.25} = 1.42$), whereas the periodic configurations (*Number* in Table 5.1) were found to be insignificant ($F = 1.06 < F_{0.25} = 1.38 < F_{0.10} = 2.04 < F_{0.05} = 2.53$). Insufficient statistical evidence was noted for the interaction between the methods and configurations (*Interaction* in Table 5.1); specifically, the performance of the debonding-control methods was not influenced by the configuration details within a 75% confidence interval.

Table 5.1 Analysis of Variance for debonding-control methods at variable significance levels

Source of variation	Sum of squares	Degrees of freedom	Mean square	F	Critical limit					
					$F_{0.05}$		$F_{0.10}$		$F_{0.25}$	
					Value	Sig	Value	Sig	Value	Sig
Methods	305.46	2	150.73	156.67	3.15	S	2.39	S	1.42	S
Number	4.07	4	1.02	1.06	2.53	I	2.04	I	1.38	I
Interaction	8.29	8	1.04	1.08	2.10	I	1.77	I	1.32	I
Error	57.73	60	0.96	-	-	-	-	-	-	-
Total	371.54	74	-	-	-	-	-	-	-	-

Methods = debonding-control methods; Number = number of grooves, U-wraps, and SMP zones (functional periodicities); Interaction = interaction between methods and numbers; Sig = significance; I = insignificant; S = significant

5.2 Inference with t -test

To complement the ANOVA-based statistical observations concerning a lump-sum evaluation, another inference technique called t -test was conducted to further examine the effects of the periodic configurations.

$$t = \frac{\bar{x} - \mu}{s / \sqrt{n}} \quad (I.2)$$

where s and n are the standard deviation and the sample number of the selected debonding-control method, respectively. It should be noted that a t -test is useful to infer statistical characteristics when the number of samples is small ($n < 30$). The hypotheses established in the ANOVA test were adopted at the same significance levels for consistency. Figure 5.1(a) compares the t values of each configuration against critical limits for the load-carrying capacity. The t values of the PG and PU categories were positioned near the limit of $\alpha = 0.10$ ($t_{critical} = 1.533$), which intimates that the individual configurations of these debonding-control methods influenced their performance (that is, load-carrying capacity) relative to the plain-bonding of the control category. In contrast, configuration of the PS category was not influential in the considered significance levels. Regarding the t values related to interfacial fracture energy (Figure 5.1(b)), the PG and PU categories exhibited similar responses as before despite the increased scatter, while the PS category tended to be statistically significant at $\alpha = 0.10$ and 0.25 .

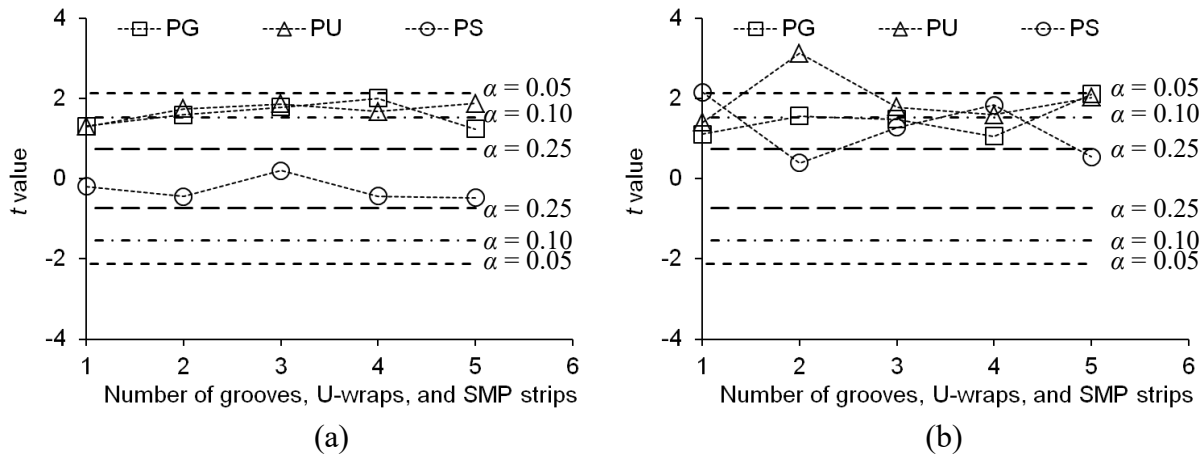


Figure 5.1 t -test results for configuration of debonding-control methods: (a) load-carrying capacity; (b) interfacial fracture energy

5.3 Evaluation of Error in Hypotheses

An error may exist in the above-described statistical assessment because of the limited replication ($n = 5$ in each test category). A probability-based evaluation was conducted to determine the level of error (β) associated with each debonding-control method (Montgomery 2013).

$$\beta = \Phi\left(z_{\alpha/2} - \frac{\delta\sqrt{n}}{\sigma}\right) - \Phi\left(-z_{\alpha/2} - \frac{\delta\sqrt{n}}{\sigma}\right) \quad (I.3)$$

$$\delta = \left| \bar{x} - \mu \right| \quad (I.4)$$

$$d = \frac{\delta}{\sigma} \quad (I.5)$$

where z is the standard normal distribution; σ is the standard deviation of the samples; and d is the characteristic parameter. The physical meaning of Eq. I.3 includes the probability of accepting an incorrect hypothesis H_0 (that is, failing to reject H_0 although it is false). Figure 5.2 plots operating characteristic curves for the F and t statistics to quantify the level of error (β) with the average d values of the test categories. As the level of significance (α) increased, the probability of detecting errors went up in F and t cases (Figure 5.2(a) and (b), respectively). In accordance with the computed error levels, the probability of correctly rejecting the hypothesis H_0 was attained ($k = 1 - \beta$) and summarized in Table 5.2. For the F statistics, the k probability of the PG and PU groups varied from 63.6% to 90.1% depending on the level of significance; however, the probability of the PS category was as low as 7.2%. These observations are attributed to the lump-sum nature of the F -based assessment and to the analogous load-carrying capacities between the PS and COT specimens. Regarding the t statistics, the PG and PU categories demonstrated 100% probabilities, meaning that the t -test results stated above were correctly generated from a probability standpoint. The PS category, however, showed relatively low k probabilities (25.3% to 64.8%) for the same reason as the F -statistic case.

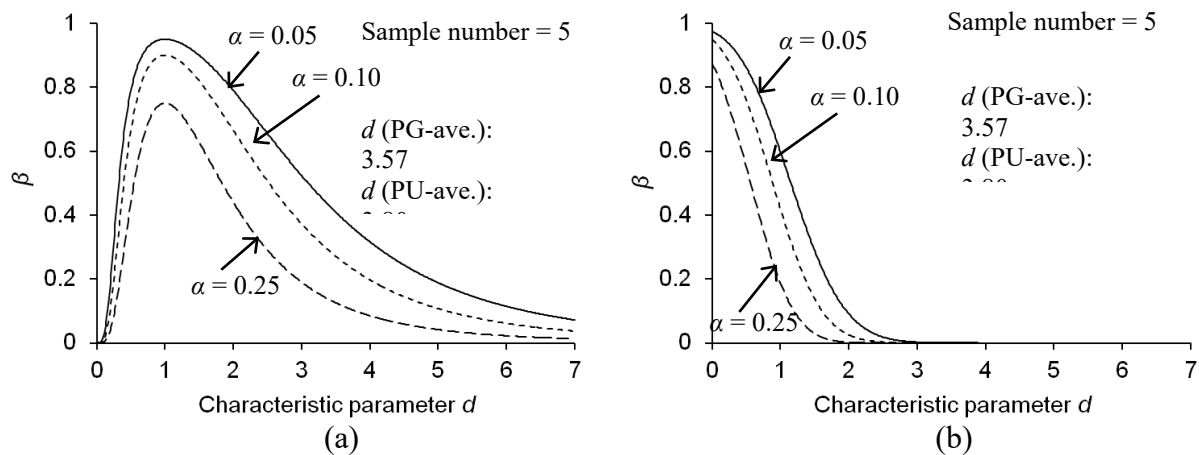


Figure 5.2 Operating characteristic curve: (a) for F statistics; (b) for t statistics

Table 5.2 Probability of correctly rejecting false H_0 hypothesis

Category	d (ave.)	F statistics			t statistics		
		$\alpha = 0.05$	$\alpha = 0.10$	$\alpha = 0.25$	$\alpha = 0.05$	$\alpha = 0.10$	$\alpha = 0.25$
PG	3.73	63.6%	76.6%	89.5%	100%	100%	100%
PU	3.80	64.9%	77.6%	90.1%	100%	100%	100%
PS	0.76	7.2%	13.6%	30.8%	25.3%	40.1%	64.8%

α = significance level

d (ave.) = average characteristic parameter

6. SUMMARY AND CONCLUSIONS

This paper investigated feasibility of a novel debonding-control concept based on functional periodicity for concrete members strengthened with CFRP sheets. Three types of stress reducers were repeatedly placed along the CFRP-concrete interface to periodically interrupt the progression of interfacial stresses: epoxy-filled grooves (PG), discrete U-wraps (PU), and silyl-modified polymer (SMP) strips (PS). Various technical aspects related to integrity of the interface were of interest, such as mechanical responses, failure modes, fracture energy, and strain development. Overall, the interfacial stresses were alleviated by the proposed approaches and CFRP-debonding was controlled. The test categories were statistically characterized and probabilistically appraised with a focus on the configuration of the periodic stress reducers. The following conclusions were drawn.

- Interfacial capacity of the PG and PU specimens was 50%-60% higher than that of the control case (COT). The number of grooves and U-wraps influenced degree of the capacity increase by mitigating propagation of the interfacial stress. As the number of the grooves and U-wraps increased, failure mode of the specimens shifted from debonding to fiber-rupture owing to the enhanced stress transfer mechanism from the CFRP to the concrete substrate (stress distribution).
- Although the PS category did not show a capacity improvement and failed by debonding, its energy absorption was noticeable due to the SMP's permanent elastic nature. Accordingly, the SMP-epoxy hybrid bond may be usable with other debonding-control schemes, which appears to be beneficial in seismic strengthening.
- Placing the grooves and U-wraps brought about a significant increase in fracture energy over 451% and 228%, respectively, relative to the control specimens. The groove and U-wrap near the loaded-end dissipated a substantial amount of energy, thereby impeding propagation of the interfacial stress toward the next grooves and U-wraps. Because of the fiber direction in the U-wraps (perpendicular to the longitudinal CFRP), strain fluctuation was recorded in the PU specimens. Partially failed SMP strips affected stress transfer to the adjacent epoxy-bonded zones.
- The lump-sum-based statistical assessment (Analysis of Variance) substantiated that debonding-control schemes influenced load-carrying capacity of the CFRP-concrete interface. The individual-based *t*-test showed that the periodic configurations of those schemes (the number of the stress reducers) were statistically significant in terms of the interfacial performance, supported by the probabilistically generated operating characteristic curves.

7. REFERENCES

- ACI. 2017. Guide for the design and construction of externally bonded FRP systems for strengthening concrete structures (ACI440.2R-17), American Concrete Institute, Farmington Hills, MI.
- Baky, H.A., Ebead, U.A., and Neale, K.W. 2007. Flexural and interfacial behavior of FRP-strengthened reinforced concrete beams, *Journal of Composites for Construction*, 11(6), 629-639.
- Eftkhar, M.R. and Ya'ghubi, M. 2016. Using boring to postpone debonding of CFRP-composite concrete beams, *Journal of Composites for Construction*, 20(1), 04015035
- Kim, Y., Quinn, K., Ghannoum, W.M., and Jirsa, J.O. 2014. Strengthening of reinforced concrete T-beams using anchored CFRP materials, *ACI Structural Journal*, 111(5), 1027-1035.
- Lee, J. and Lopez, M.M. 2016. Characterization of FRP Uwrap anchors for externally bonded FRP-reinforced concrete elements: an experimental study, *Journal of Composites for Construction*, 20(4), 04016012.
- Montgomery, D.C. 2013. Design and analysis of experiments (8th edition), Wiley, Hoboken, NJ.
- Mostofinejad, D. and Mahmoudabadi, E. 2010. Grooving as alternative method of surface preparation to postpone debonding of FRP laminates in concrete beams, *Journal of Composites for Construction*, 14(6), 804-811.
- Smith, S.T. and Teng, J.G. 2001. Interfacial stresses in plated beams, *Engineering Structures*, 23, 857-871.
- Wu, Y.-F., He, L., and Bank, L.C. 2016. Bond-test protocol for plate-to-concrete interface involving all mechanisms, *Journal of Composites for Construction*, 20(1), 04015022.

PART II: Debonding-Mitigation of CFRP-Strengthened RC Beams with Grooved Bonding

8. INTRODUCTION

Structural strengthening with carbon fiber reinforced polymer (CFRP) sheets is common practice in the rehabilitation community, with a number of benefits such as high strength, outstanding durability, low density, easy application, and minimal maintenance expense (ACI 2007). Premature debonding or delamination of CFRP sheets from the concrete substrate is, however, recognized as a salient problem. Once local bond failure initiates and progresses, capacity of the strengthened members conspicuously decreases (Ceroni et al. 2008). Accordingly, debonding usually dominates the design of CFRP-strengthening, rather than the constituents' strength. The majority of design guidelines restrict usable stress or strain of externally-bonded CFRP (called *effective stress* or *strain*) to avoid premature bond failure (AASHTO 2012; ACI 2017), which does not seem efficient in fully utilizing the high strength of CFRP materials (Kalfat and Al-Mahaidi 2011). To overcome these limitations of ordinary CFRP-bonding implemented on a plain substrate, anchorage may be installed. U-wrap anchors are often bonded near the ends of longitudinal CFRP sheets to inhibit peeling failure, whereas the anchors are prone to bond degradation with a local slip (Ceroni, et al. 2008; Colalillo and Sheikh 2014). Non-traditional anchor systems, expected to address the potential problems of U-wraps, involve fan-type fibers (Al-Sammari and Brena 2018; Garcia et al. 2018), transverse rods winding the termination of CFRP sheets (Khalifa et al. 1999), and plates with mechanical fasteners (El-Maaddawy and Chekfeh 2012). Most of these anchors are intended for shear-strengthening and may not be conveniently useable for flexural-strengthening.

Rather than placing physical anchorage, alternative approaches were recently attempted by modifying concrete substrates. Mostofinejad and Mahmoudabadi (2010) cut diagonal slits (2 mm (0.08 in.) deep) on the tensile soffit of concrete prisms prior to bonding CFRP sheets. The surface-prepared specimens were then monotonically loaded to examine the behavior of the CFRP-concrete interface. The slit prisms showed an increase in the load-carrying capacity over 15% relative to those without surface preparation. Eftkhar and Ya'ghubi (2016) experimented with the validity of multiple holes (diameter = 8 mm (0.3 in.) to 16 mm (0.6 in.)) drilled into a concrete substrate, along which CFRP sheets were adhered by a bonding agent. The purpose of drilling was to facilitate stress transfer between the concrete and CFRP. In spite of CFRP-debonding, the capacity of the holed prisms was 35% higher than that of a plain prism along with increased ductility. Sui et al. (2018) carried out pull-out tests using concrete prisms bonded with CFRP sheets. The substrate had narrow grooves in the lateral direction of the prism at a depth and spacing of 5 mm (0.2 in.) and 10 mm (0.4 in.), respectively, and filled with either cementitious and epoxy resins. The performance of the epoxy-filled prisms was better in terms of bond capacity, interfacial slip, and energy dissipation.

Review of the relevant literature, albeit insufficient at this time, manifests that the explicitly treated substrate of a concrete member for CFRP-strengthening can improve the integrity of the CFRP-concrete interface without anchorage. It is, however, unknown that the preliminary results from small unreinforced concrete prisms (400 mm (16 in.) to 500 mm (20 in.) in length) are applicable to actual structural members. This paper studied the potential of grooved substrates filled with an epoxy adhesive for debonding control of reinforced concrete beams strengthened with CFRP sheets. An experimental program was conducted to elucidate the effects of various bonding schemes on the load-carrying capacity, failure mechanisms, and flexural behavior of the strengthened beams. Analytical modeling further clarifies stress transfer from the substrate to the bonded sheets at the local and global levels.

9. RESEARCH SIGNIFICANCE

Due to the inherent weak-link between the concrete substrate and externally-bonded CFRP, delamination can be highly likely during the service life of strengthened members. The bond performance of CFRP is enhanced by anchor systems, whereas there is a dearth of consensus on the employment of anchorage among practitioners. The strengthening design was, consequently, performed with either case-specific anchors or a conservative amount of CFRP materials to reduce effective strains, which warrants the need for additional research in debonding control to fundamentally reframe existing practices. A new concept for grooved CFRP-bonding is proposed and tested with the aim of achieving a sustainable CFRP-concrete interface.

10. EXPERIMENTAL PROGRAM

The following outlines materials, preparation, specimens, test setup, and instrumentation. Emphasis is placed on non-conventional bonding systems for CFRP sheets.

10.1 Materials

Concrete was mixed with a specified compressive strength of 20 MPa (2,900 psi), which can represent the condition of decrepit concrete structures (CSA 2014). The average strength of cylinders, tested in accordance with ASTM C39 (ASTM 2018), was 19 MPa (2,800 psi) with a standard deviation of 0.7 MPa (100 psi). Steel cages were fabricated using two longitudinal No. 3 bars (cross-sectional area = 71 mm² (0.11 in.²), each) with 90° hooks at both ends to avoid slippage and using No. 2 shear stirrups (cross-sectional area = 32 mm² (0.05 in.²), each) spaced at 75 mm (3 in.). CFRP sheets were made of unidirectional carbon fabrics and an epoxy matrix based on wet-layup. According to the manufacturer, the sheet had a tensile strength of 3,800 MPa (550 ksi), an elastic modulus of 227 GPa (33,000 ksi), a rupture strain of 0.0167, and an equivalent fiber thickness of 0.165 mm (0.006 in.). The epoxy resin (mixture of a resin and a hardener) had a nominal tensile strength of 55 MPa (8 ksi) with an elastic modulus of 3 GPa (440 ksi) and a Poisson's ratio of 0.4.

10.2 Beam Preparation

Eight reinforced concrete beams (100 mm (4 in.) wide by 165 mm (6.5 in.) deep by 1,200 mm (47 in.) long, Figure 10.1) were cast and cured for 28 days in a humidity room. After cleaning with a compressed air, the tensile soffit of the beams was cut using an electric saw in the transverse direction to create grooves, as illustrated in Figure 10.1(a) (strengthening schemes are detailed in the subsequent section). The size of each groove was 15 mm (0.6 in.) by 20 mm (0.8 in.). Prior to bonding the CFRP sheets, the surface of the beams was roughened using an electric grinder to improve bond performance.

10.3 Strengthening Details

The purpose of creating periodic grooves, to be filled with the two-part epoxy, was to alleviate interfacial stresses along the bond-line. Literature reports that normal stresses incurring the peel-off failure of CFRP are reduced with an increase in adhesive thickness (Taljsten 1997). The epoxy components were mixed at a resin-to-hardener ratio of 3:1 by mass and pasted along the concrete substrate, followed by the impregnation of precut carbon fabric (100 mm (4 in.) wide by 900 mm (35 in.) long). The adhesive was additionally applied as a topcoat to fully cover the fabric, so a single layer of CFRP composite sheet was accomplished. Four categories were tested to evaluate efficacy of the grooved bonding scheme, as listed in Table 10.1. The unstrengthened control beam was designated to be UNS. The identification code of the strengthened beams signified groove configurations and a distance from the CFRP termination point to the nearest groove, which are graphically explained in Figure 10.1(b). The CG0 beam was strengthened without grooves (that is, plain-bonding of CFRP). The CG3 series had three grooves near the CFRP termination where a stress concentration takes place. The epoxy-filled grooves were intended to mitigate stress development, thereby delaying delamination failure. To examine the degree of stress control, the location of the nearest groove was shifted by 0 mm (0 in.) to 100 mm (4 in.) from the termination point (CG3-0 to CG3-100 in Table 10.1). The CGD beams were strengthened with distributed grooves along the span to preclude intermediate-crack-induced debonding (IC-debonding, hereafter) and to lower stresses in the vicinity of the CFRP termination. Complying with the manufacturer's recommendation, the strengthening system was cured for seven days at room temperature.

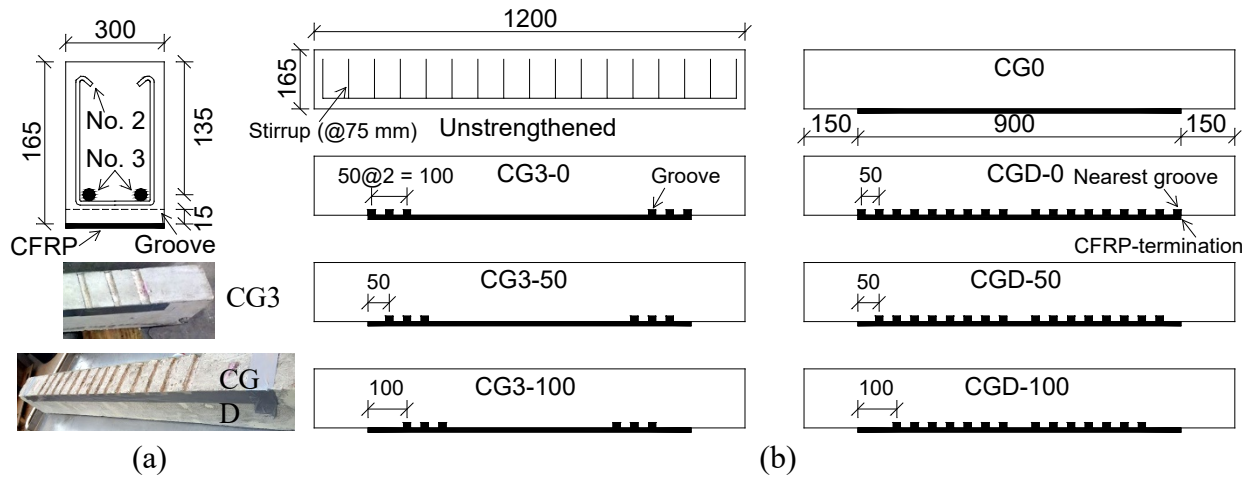
Table 10.1 Test matrix [1 mm = 0.0394 in.; 1 kN = 0.225 kip]

Beam ID	Groove characteristic		Ultimate load (kN)	Failure sequence ^c
	Configuration ^a	Distance (mm) ^b		
UNS	Unstrengthened	-	47.2	FC→SC→CC
CG0	0 grooves	-	57.1	FC→SC→CD→PD→CC
CG3-0	3 grooves	0 mm	64.9	FC→SC→CD→PD→CC
CG3-50	3 grooves	50 mm	64.2	FC→SC→CD→PD→CC
CG3-100	3 grooves	100 mm	63.9	FC→SC→CD→PD→CC
CGD-0	Distributed	0 mm	72.1	FC→SC→LD→SF
CGD-50	Distributed	50 mm	69.8	FC→SC→LD→SF
CGD-100	Distributed	100 mm	65.3	FC→SC→LD→SF

^a: 0 grooves = plain CFRP-bonding; 3 grooves = 3 grooves near CFRP termination; Distributed = distributed grooves along CFRP

^b: Distance = distance from CFRP-termination to nearest groove

^c: FC = flexural crack; SC = shear crack; CC = concrete crushing; CD = CFRP delamination; PD = progression of delamination; LD = local disintegration of CFRP at termination; SF = shear failure accompanied by concrete crushing



[1 mm = 0.0394 in.]

Figure 10.1 Beam details (units in mm): (a) dimension and grooves; (b) strengthening schemes

10.4 Test Setup

The strengthened beams were monotonically loaded under four-point bending, as shown in Figure 10.2(a), at a rate of 2 mm/min (0.08 in./min) until failure. To avoid stress concentrations, a steel strip was placed beneath each loading point. The applied load and the displacement at midspan were measured by a load cell and a linear potentiometer, respectively. Displacement-type strain transducers (PI gages) were installed at a distance of 25 mm (1 in.) from the top and bottom of the beams (Figure 10.2(b)) to log development of tensile and compressive strains. Six strain gages were bonded along the CFRP sheet at a spacing of 50 mm (2 in.) to understand the failure mechanism of the grooved interface (Figure 10.2(a)). The full-field deformation and cracking pattern of the individual beams, adjacent to the CFRP-termination, was examined by a digital image correlation (DIC) technique (Figure 10.2(c)). The high-resolution camera provides 5.0 Megapixel images (2,448 by 2,048), which are analyzed by the data acquisition computer equipped with a 16 GB RAM and a quad-core 3.5 GHz processor. The monitored region was in the shear span of the respective beams, in which the failure of the strengthening system would occur. One side of the shear span was painted in white to augment the quality of digital images (Figure 10.2(c), inset).

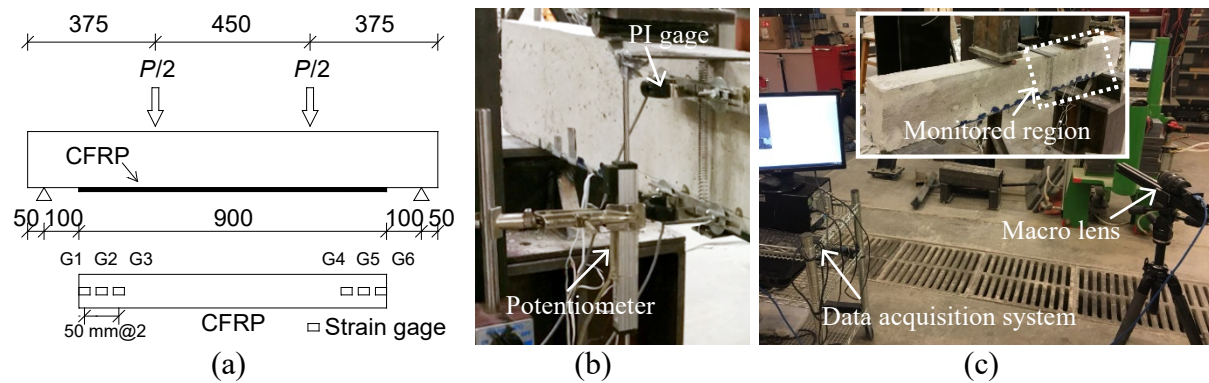


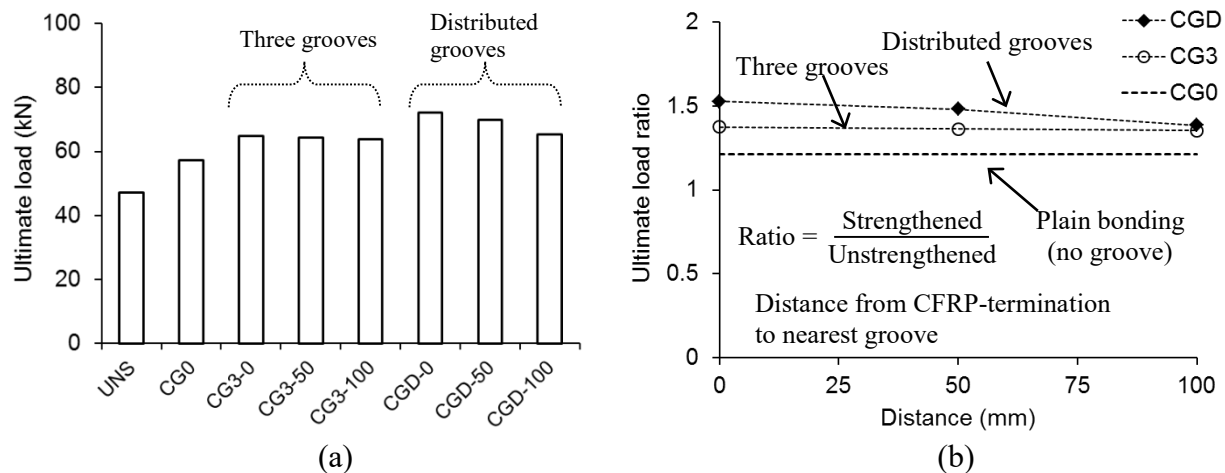
Figure 10.2 Test setup and instrumentation: (a) loading scheme (units in mm [1 mm = 0.039 in.]); (b) potentiometer and PI gages; (c) digital image correlation (DIC) technique

11. TEST RESULTS

Based on the application of groove-bonding, experimental findings were delineated with the flexural capacity and behavior of CFRP-strengthened beams. The failure mechanism was comprehended beside the progression of concrete cracking and CFRP-delamination.

11.1 Beam Capacity

The load-carrying capacity of the beams is shown in Figure 11.1(a). The unstrengthened control beam (UNS) failed at a load of 47.2 kN (10.6 kips), which was 23.3% lower than the ultimate load of the beam with plain CFRP-bonding (CG0). As the grooves were present, capacity of the beams markedly improved. In comparison with the UNS beam, the beams with three grooves (the CG3 series) and with distributed grooves (the CGD series) exhibited average increases of 36.3% and 46.3% in the capacity, respectively. The distance between the CFRP termination and the nearest groove was influential on the capacity variation. For clarity, ultimate loads of the strengthened beams were normalized by that of the unstrengthened beam (that is, *ultimate load ratio* in Figure 11.1(b)). Ratios of the three-grooved beams (CG3) were almost invariant, meaning that progression of peeling stresses near the CFRP termination was effectively controlled; as such, the occurrence of delamination failure was postponed (to be detailed). On the contrary, ratios of the CGD beams with distributed grooves dwindled with an increase in the distance between the CFRP termination and the nearest groove. For example, the comparison ratios were 1.53 and 1.38 for the beams with distances of 0 mm (CGD-0) and 100 mm (CGD-100), respectively. Performance of the CGD beams was more susceptible to the groove configurations than that of the CG3 beams, although the former's capacities were consistently higher.



[1 kN = 0.225 kip; 1 mm = 0.0394 in.]

Figure 11.1 Load-carrying capacity: (a) individual comparison; (b) effect of groove configuration

11.2 Failure Mode

Pictured in Figure 11.2 are the failure modes of the beams. Typical flexural and shear (diagonal tension) cracks were observed in the UNS beam (Figure 11.2(a)). Average spacing of the flexural cracks in the constant moment zone was 87 mm (3.0 in.), which reasonably agrees with a stabilized-crack spacing of 93 mm (3.7 in.) predicted by CEB-FIP (1993). Multiple shear cracks formed and propagated toward the loading points; afterward, the test was ceased when the concrete crushed. CFRP-delamination was the

primary failure of the CG0 beam (Figure 11.2(b)), while concrete-crushing was secondary. Instead of showing traditional end-peeling failure, which involves a sudden load-drop (Pham and Al-Mahaidi 2004), the delamination occurred at one of the CFRP-termination points and steadily evolved at the rebar level with the increased load. It should be noted that one side of the beam was marked for tracking the growth of the cracks, whereas the other side was used for DIC-imaging. The failure of the CG3 series (Figure 11.2(c)) was attributed to cover-delamination, analogous to that of the CG0 beam. Nonetheless, the average failure load of the former was higher by 36.3%, as discussed previously. This fact substantiates the effectiveness of the grooved bonding scheme on mitigating stresses near the CFRP-termination. Specifically, two types of stresses are associated (normal and shear, Taljsten 1997) to bring about the delamination of CFRP. Regarding beams with the distributed grooves, a different failure mode was noticed (Figure 11.2(d)). The onset of CFRP-delamination was observed at one of the termination points, like other beams; however, the delamination was not progressed. As the flexural load increased, shear cracks initiated and grew, eventually leading to the failure of the beams. The distributed grooves interrupted development of flexural cracks, because the periodic epoxy-filled grooves carried tensile stresses and restrained the concrete deformation (supplementary information to follow in a subsequent section).

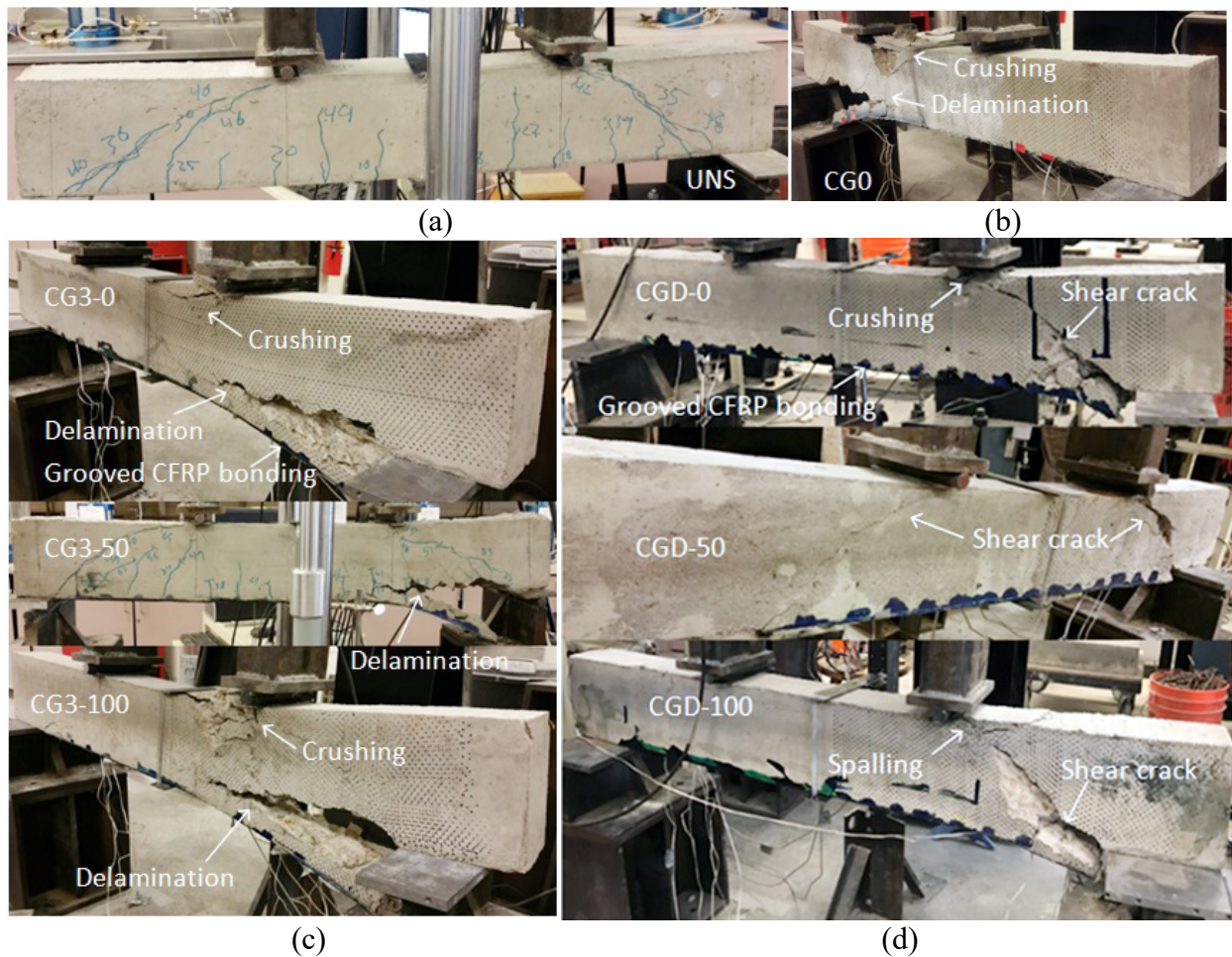
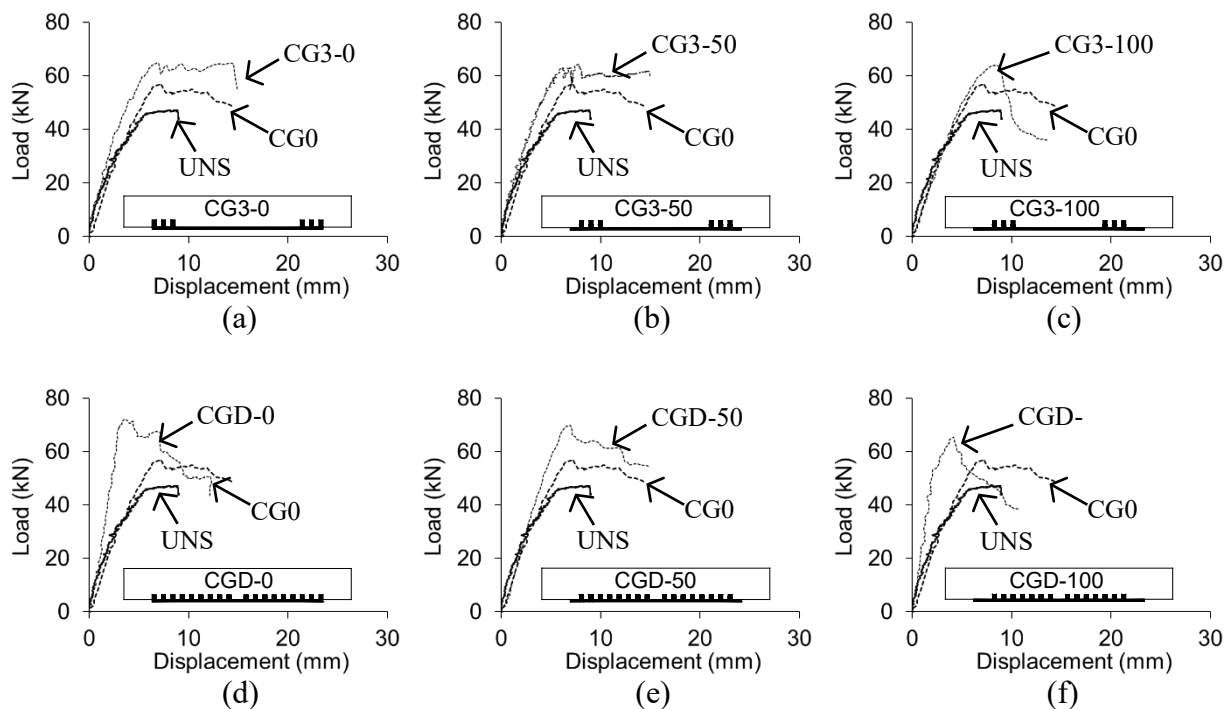


Figure 11.2 Failure modes: (a) unstrengthened beam (UNS); (b) strengthened beam with grooves (CG0); (c) strengthened beams with three grooves on both sides (CG3); (d) strengthened beams with distributed grooves (CGD)

11.3 Flexural Behavior

Figure 11.3 comparatively assesses load-displacement behavior of the grooved beams relative to that of the unstrengthened (UNS) and plain-CFRP (CG0) beams. There was a marginal difference in pre-yield stiffness between the UNS and CG0 beams (Figure 11.3(a)), which indicates that the conventional plain CFRP-bonding was not efficacious from a serviceability standpoint. This is well-recognized in the rehabilitation community because the purpose of CFRP-strengthening is not to upgrade the serviceability of a flexural member, but to increase the load-carrying capacity (prestressed CFRP sheets should be employed when simultaneously addressing serviceability and strength, El-Hacha et al. 2001). Unlike typical CFRP-strengthened beams showing an abrupt load-drop immediately after end-peeling failure (Pham and Al-Mahaidi 2004), the CG0 beam revealed a gradually decreasing post-peak load owing to the progressive delamination of CFRP, as elaborated in the failure mode section. The fact that the in-service stiffness of the CG3-0 beam was higher than its CG-0 counterpart (Figure 11.3(a)) can be explained by the pseudo-anchorage effect resulting from grooves at both ends of the CFRP sheet. In other words, these grooves resisted horizontal deformation of the adhesive layer when the curvature of the beam increased, as though the longitudinal CFRP sheet was anchored at the ends. With an increase in distance between the CFRP termination and the nearest groove, the anchorage effect decayed (Figure 11.3(b) and (c) for the CG3-50 and CG-100 beams, respectively); furthermore, the extent of a load-drop beyond the peak loads became conspicuous (Figure 11.3(a) to (c)). The location of the grooves was, therefore, found to be influential on the pre- and post-peak responses of the CG3 beams.



[1 kN = 0.225 kip; 1 mm = 0.039 in.]

Figure 11.3 Load-displacement of beams: (a) CG3-0; (b) CG3-50; (c) CG3-100; (d) CGD-0; (e) CGD-50; (f) CGD-100

The behavior of the CGD beams is plotted in Figure 11.3(d) to (f). The distributed grooves noticeably improved the pre-yield stiffness of the beams, which carried tensile stresses and controlled flexural cracks that reduced the moment of inertia of the beams, although the CGD-50 beam exhibited a relatively lower stiffness due to the cracks in both shear spans (the CGD-0 and CGD-100 beams had shear cracks in a single span, Figure 11.2(d)). Consistent with the post-peak behavior of the CG3 series, the CGD-0 and CGD-50 beams demonstrated a similar load-drop pattern after the peak loads (Figure 11.3(d) and (e)), while the CGD-100 beam showed a rapid drop (Figure 11.3(f)). These observations signify that stress development near the CFRP-termination was reliant upon the local interaction between the CFRP and the cover concrete, rather than on the configuration of the far-field groove configurations (away from the termination).

The tensile and compressive strains at midspan of selected beams are provided in Figure 11.4 (CG3-50 and CGD-50 were compared with UNS for brevity, since these grooved beams were sufficient to explain efficacy of the proposed bonding schemes). Notwithstanding slight differences, the compressive strains of these three beams were akin, implying that the influence of the grooved bond was modest above the neutral axis of the beams. As per transformed section theory, the neutral axis depths of the UNS and CG3/CGD beams at midspan were calculated to be 86 mm (3.39 in.) and 87 mm (3.43 in.) for the uncracked section and 49 mm (1.93 in.) and 52 mm (2.05 in.) for the cracked section, respectively. Tensile strain of the grooved beams was less than that of the unstrengthened beam at the same load level, particularly for the CGD-50 case. That is, the CFRP-bonding schemes impeded the sectional rotation at midspan, related to the local curvature of the strengthened beams, which differs from the aforementioned midspan displacement (Figure 11.3) influenced by the occurrence of shear cracks.

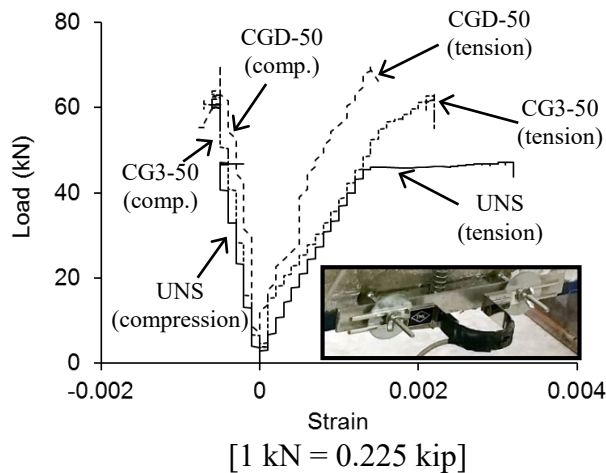
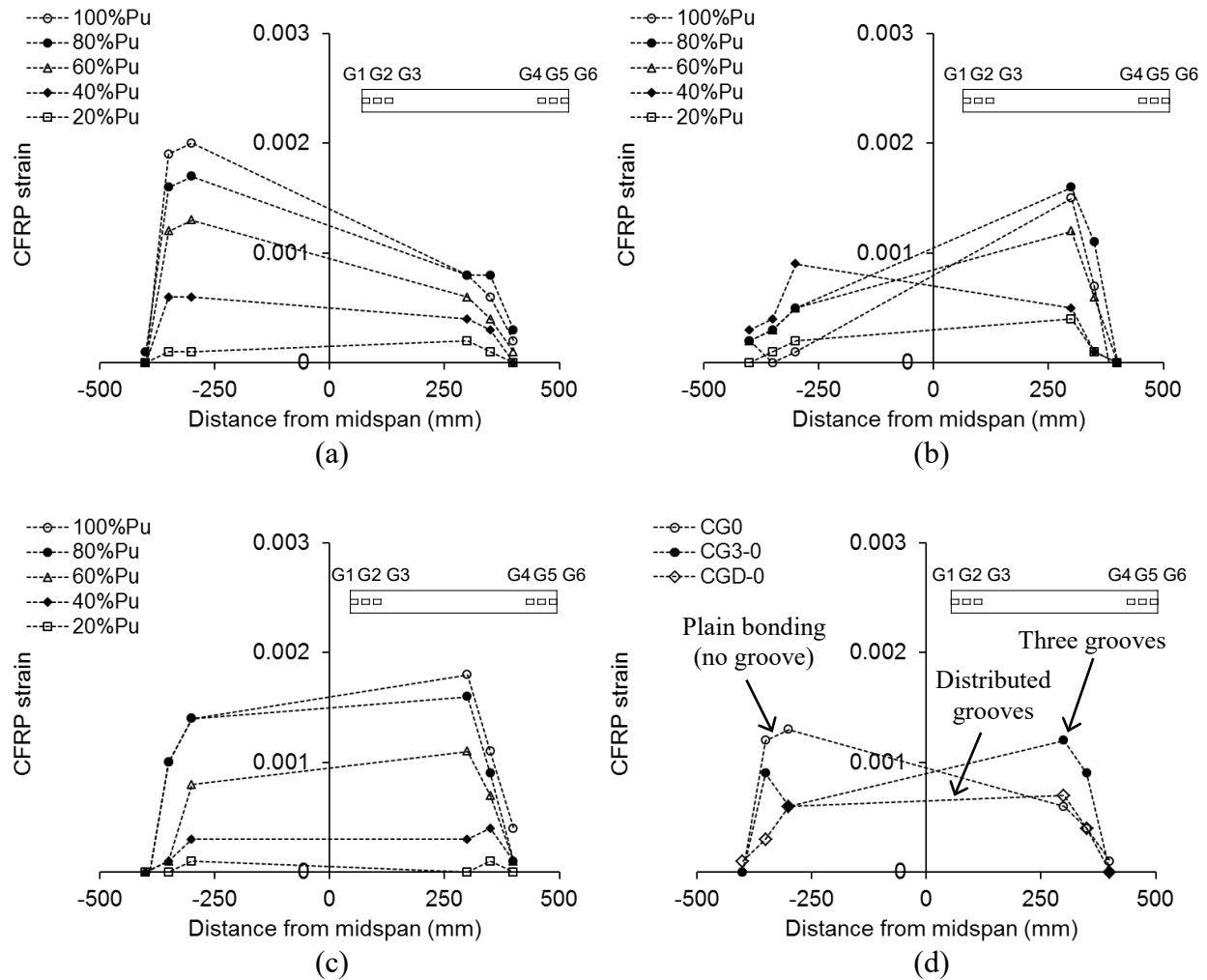


Figure 11.4 Load-strain behavior at midspan

11.4 Profile of CFRP Strain

The strain profile of CFRP is available in Figure 11.5, depending on a load level normalized by the flexural capacity of each beam, P_u . For the plain-CFRP beam (CG0, Figure 11.5(a)), the strain development was reasonably symmetric up to a load level of $40\%P_u$, beyond which the increment of the left side (G1 to G3) was pronounced because the other side (G4 to G6) experienced cracking associated with the progressive delamination that hindered a stress transfer from the concrete to the CFRP. For this reason, the strain values of G5 and G6 at $100\%P_u$ were lower than those at $80\%P_u$. The trend of strain development in the CG3 series was intricate, as shown in the case of CG3-100 (Figure 11.5(b), this beam that failed at a lower load than others in the CG3 series was selected to discuss the adverse strain responses). The interfacial integrity near the CFRP-termination was preserved up to a load level of $40\%P_u$; however, the grooved region on the G1 side was subjected to irregular stresses above $60\%P_u$ because of the local cracking that brought about unstable strain variations and eventually led to the delamination failure. Contrary to the steady increase of G4 to G6, the strains of G1 to G3 dropped with the load due to the impaired CFRP-concrete interface. The failure of the interface on one side (G1 to G3) partially affected the deformation of the interface on the other side along the bond-line, so that the strains of G4 to G6 at $100\%P_u$ were lower than those at $80\%P_u$. Such a finding is proposed to be called the *released strain tensility* of the interface.

The strain conformation of the uniformly grooved beam was stable (Figure 11.5(c), CDG-100 was adopted for consistency with CG3-100) at all load levels, compared with that of the other beams, which reaffirms the favorable performance of the proposed bonding scheme in terms of upholding interfacial integrity. Figure 11.5(d) appraises the profile of CFRP strains taken from the CG3-0 and CGD-0 beams at $60\%P_u$ of the CG0 beam, representing a typical service load level. These beams demonstrated higher load-carrying capacities than other beams in their respective test categories (Table 10.1); accordingly, the comparison in Figure 11.5(d) can provide a proper evaluation on the interfacial behavior of the grooved beams under service loading. The strain patterns of CG3-0 and CG0 were alike and asymmetric, as explicated above, which are distinguishable from the balanced pattern of CGD-0. The lower strains of CGD-0 denote that the applied tensile stresses were efficaciously distributed along the interface; as a result, the cracking resistance of the beam and its flexural stiffness were enhanced.



[1 mm = 0.039 in.]

Figure 11.5 CFRP strain profile: (a) CG0; (b) CG3-100; (c) CDG-100; (d) comparison at 60% P_u of CG0

11.5 Progression of Delamination and Cracking

Figure 11.6 renders DIC-based assessments on the progression of CFRP-delamination and cracking in the grooved beams at near-failure states (for conciseness, representative beams were chosen and compared). The delamination of the CG3-0 beam initiated at a load level of 82% P_u in line with one of the shear cracks, as shown in Figure 11.6(a). Several secondary cracks were noticed in the shear span. The cover-level delamination and the secondary cracks became prominent at 96% P_u , and finally the beam failed by the complete regional delamination and concrete crushing at 100% P_u . Geometric discontinuity of the concrete due to the presence of steel bars inside the beam caused stress concentrations, which guided propagation of the cover delamination. As far as the distributed grooves are concerned (Figure 11.6(b)), the initiation of the delamination in CGD-50 was observed at 92% P_u (a higher load level than the three-grooved beam owing to the retarded stress transfer along the CFRP-concrete interface). Passing through the local disintegration of the interface at 97% P_u , the beam failed as a result of shear cracks without cover-delamination at 100% P_u . The distributed grooves alleviated the growth of tensile stresses in the beam, as expounded earlier; consequently, the extent of the rebar-level stress concentrations was insufficient to generate delamination failure, including the controlled secondary cracks.

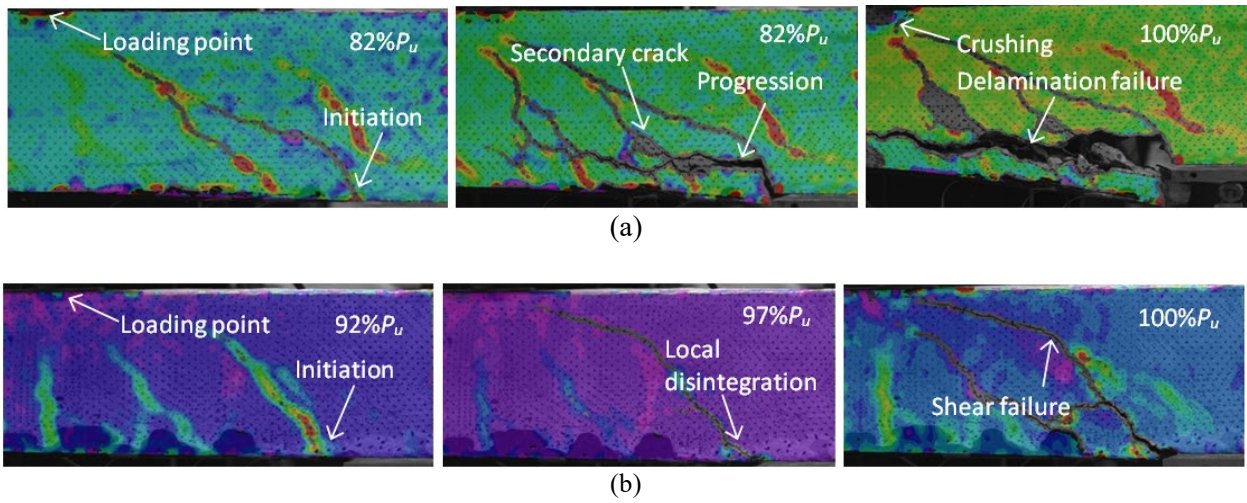


Figure 11.6 Crack development: (a) strengthened beam with three grooves on both sides (CG3-0); (b) strengthened beam with distributed grooves (CGD-50)

12. MODELING OF STRESS TRANSFER

From interfacial and structural points of view, analytical modeling is presented to account for the characteristics of groove-bonded CFRP. The focus is on the integrity of CFRP-concrete interface and the effects of variables constituting the strengthening system.

12.1 Local Response by Interfacial Shear

Model—Interfacial shear stress, $\tau(x)$, for a CFRP-strengthened beam under four-point bending may be obtained by (Smith and Teng 2001)

$$\tau(x) = A_1 \cosh(\lambda x) + A_2 \sinh(\lambda x) + m_1 (P/2) \quad (\text{II.1})$$

$$A_1 = \left(\frac{P}{2}\right) \left(\frac{m_2}{\lambda} a - m_1 e^{-\lambda(b-a)}\right) \text{ and } A_2 = -\left(\frac{P}{2}\right) \frac{m_2}{\lambda} a \quad (\text{II.2})$$

$$m_1 = \frac{G_a}{t_a} \frac{1}{\lambda^2} \left(\frac{y_1 + y_2}{E_1 I_1 + E_2 I_2}\right) \text{ and } m_2 = \frac{G_a}{t_a} \frac{y_1}{E_1 I_1} \quad (\text{II.3})$$

$$\lambda^2 = \frac{G_a b_f}{t_a} \left(\frac{(y_1 + y_2)(y_1 + y_2 + t_a)}{E_1 I_1 + E_2 I_2} + \frac{1}{E_1 A_1} + \frac{1}{E_2 A_2}\right) \quad (\text{II.4})$$

where x is the distance from the CFRP termination to any location along the interface ($0 \leq x \leq (b - a)$, in which a and b are the distances from the support to the termination and loading point, respectively); P is the total load; G_a and t_a are the shear modulus and thickness of the adhesive, respectively; y_1 and y_2 are the distances from the bottom of the beam and the top of CFRP to their centroids, respectively; E , I , and A are the elastic modulus, moment of inertia, and cross-sectional area of the beam and CFRP (subscripts 1 = beam and 2 = CFRP), respectively; and b_f is the CFRP width.

Implementation — To implement the elastic closed-form equations for the present test program, a typical load of 5 kN (1.1 kips) below the theoretical cracking load of the beam ($P_{cr} = 7.9$ kN (1.8 kips)) was applied with the following properties: $t_a = 1$ mm (0.0394 in.) (measured average), $G_a = 1.1$ GPa (160 ksi) (obtained from elastic theory using the above-mentioned elastic modulus and Poisson's ratio of the epoxy), and $E_1 = 57000\sqrt{f'_c}$ in psi or $4730\sqrt{f'_c}$ in MPa, ACI 318-14 (ACI 2014). Other geometric properties for Eqs. II.1 to II.4 were determined from the transformed section of the strengthened beams. Figure 12.1(a) illustrates the stress profiles of the CG0 and CG3-0 beams (the maximum stress of the CG3-50 and -100 beams was identical to that of CG0 owing to absence of the groove at the CFRP-termination). Compared with the CG0 beam, the CG3-0 beam revealed a 71.0% lower stress at the CFRP-termination ($x = 0$ mm (0 in.)). This accounts for the favorable role of the epoxy-filled groove in reducing the interfacial stress, which would eventually delay the delamination failure of the beam. The predicted stress of the beam with distributed grooves (CGD-0, as given in the inset of Figure 12.1(a)) was essentially the same as that of CG3-0, except for the marginal stress drops associated with the additional grooves. To examine effects of the constituent variables, parametric investigations were conducted (Figure 12.1(b) to (f)). The default properties of the CGD-0 beam, which exhibited the highest load-carrying capacity, were used, unless otherwise stated. Shown in Figure 12.1(b) are the stress variations of the beam with groove thickness. The maximum interfacial stress decreased by 52.9% to 78.3% with a groove thickness of 5 mm (0.2 in.) to 30 mm (1.2 in.), which suggests the importance of creating a groove at the CFRP-termination when a strengthening design is conducted. Development of the interfacial stress

was dependent on the moduli of the CFRP and epoxy (Figure 12.1(c) and (d)): high-modulus strengthening systems generated high stresses. In practice, low modulus CFRP sheets may not be recommendable since flexural capacity of the strengthened beam will be affected; nonetheless, a low modulus epoxy appears beneficial as long as stress transfer from the concrete substrate to the CFRP is preserved. The substrate strength did not change the interfacial stress within a range from $f'_c = 15$ MPa (2,200 psi) to 40 MPa (5,800 psi) (Figure 12.1(e)); thus, the proposed strengthening scheme can be used regardless of concrete strength. Figure 12.1(f) provides the influence of the distance between the support and the CFRP-termination. It is advisable that the termination point be as close as possible to the support in order to maintain the integrity of the interface when loaded.

12.2 Global Response by Beam Bending

Model — As per strain compatibility and force equilibrium, the following equations are obtained for any cross section of a CFRP-strengthened beam

$$C_c(x) = A_s E_s \varepsilon_s(x) + A_f E_f \varepsilon_f(x) \quad (\text{II.5})$$

$$\alpha_1 \beta_1 f'_c c(x) b = A_s E_s \frac{(d - c(x))}{c(x)} \varepsilon_c(x) + A_f E_f \frac{(h - c(x))}{c(x)} \varepsilon_c(x) \quad (\text{II.6})$$

where $C_c(x)$ is the resultant compressive force of the concrete at position x along the span; A_s and A_f are the cross-sectional areas of the steel and CFRP, respectively; $\varepsilon_s(x)$ is the steel strain ($\varepsilon_s(x) \leq \varepsilon_y$, where ε_y is the yield strain of the steel); $\varepsilon_f(x)$ is the CFRP strain; $c(x)$, b , d , and h are the neutral axis depth, width, effective depth, and height of the beam, respectively; E_s and E_f are the elastic moduli of the steel and CFRP, respectively; $\varepsilon_c(x)$ is the concrete strain at the extreme compression fiber; and α_1 and β_1 are the equivalent stress block factors for the concrete before crushing, which may be attained by (ACI 2017)

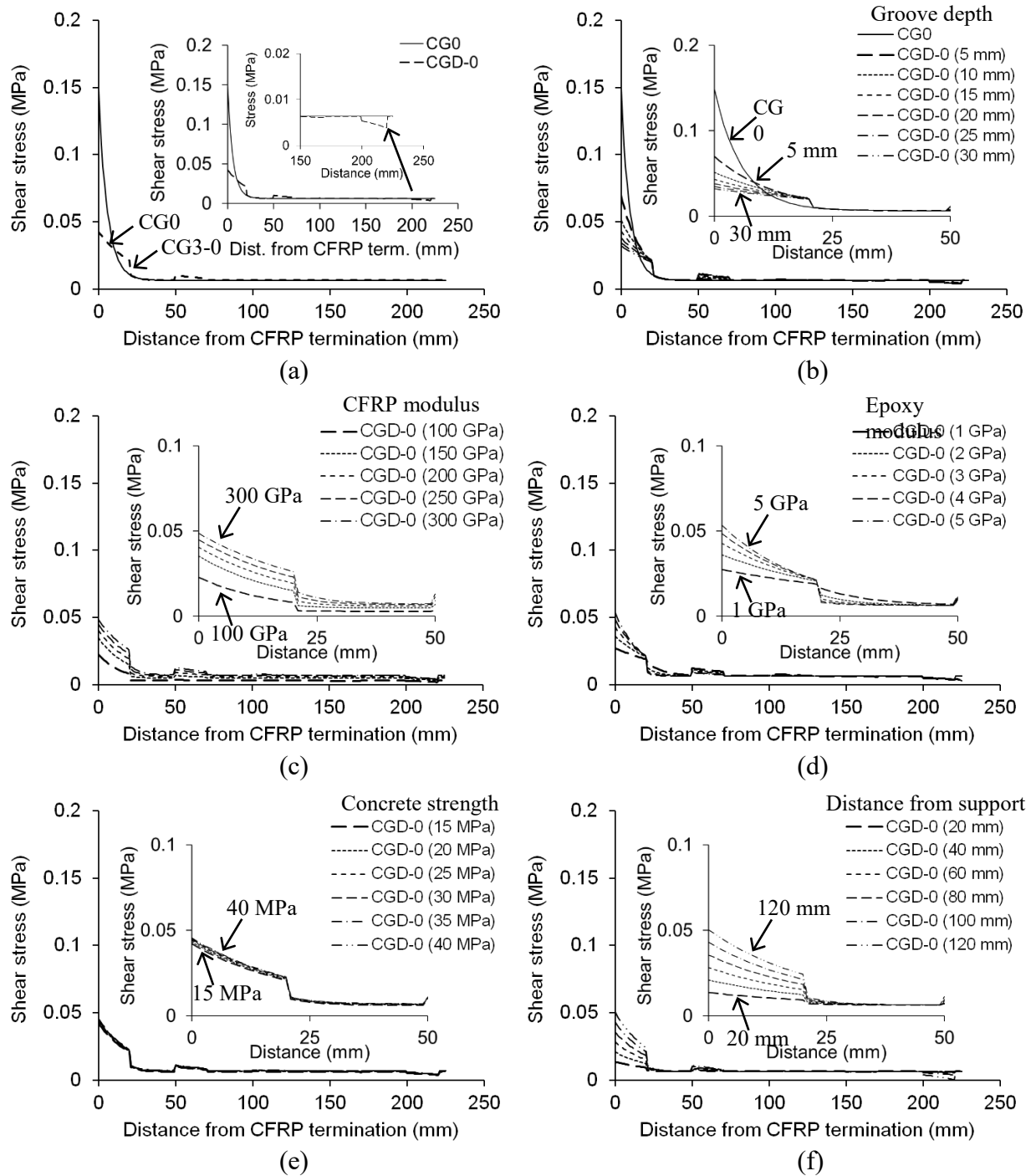
$$\alpha_1 = \frac{3\varepsilon'_c \varepsilon_c(x) - \varepsilon_c'^2(x)}{6\beta_1 \varepsilon_c'^2} \quad (\text{II.7})$$

$$\beta_1 = \frac{4\varepsilon'_c - \varepsilon_c(x)}{6\varepsilon_c'^2 - 2\varepsilon_c(x)} \quad (\text{II.8})$$

$$\varepsilon'_c = \frac{1.7f'_c}{E_c} \quad (\text{II.9})$$

where E_c is the elastic modulus of the concrete, as specified above, and $\varepsilon_c(x)$ is the concrete strain showing linear responses in the test

$$\varepsilon_c(x) = \frac{M(x)c(x)}{E_c I(x)} \quad (\text{II.10})$$



[1 mm = 0.0394 in.; 1 MPa = 145 psi; 1 GPa = 145 ksi]

Figure 12.1 Shear stress profile at a load of 5 kN (1.1 kips): (a) comparison between plain bonding with grooved bonding; (b) effect of groove depth; (c) effect of CFRP modulus; (d) effect of epoxy modulus; (e) effect of concrete strength; (f) effect of distance from CFRP termination and support

where $M(x)$ is the applied moment and $I(x)$ is the moment of inertia of the section that is calculated by the transformed section of the beam, as stated in ACI 440.2R-17 (ACI 2017), contingent on the magnitude of the moment relative to the cracking moment of the section. The moment gradient in the shear span is solved for by

$$M(x) = \frac{P'_u}{2} x \quad (\text{II.11})$$

where P'_u is the near-failure load of the beam. Equations II.5 to II.10 are iterated with a given moment (Eq. II.11) until convergence is achieved to acquire the curvature-induced steel and CFRP strains ($\varepsilon_s(x)$ and $\varepsilon_f(x)$, respectively) at the near-failure state of the beam, prior to the initiation of the delamination (strain compatibility is valid).

The Mode II energy release rate (in-plane shear) of the CFRP-concrete interface, $G_{II}(x)$, may be calculated by (Wan et al. 2004)

$$G_{II}(x) = \frac{P_f(x)^2}{2E_f t_f b_f^2} \quad (\text{II.12})$$

where $P_f(x)$ is the force applied to the CFRP sheet ($P_f(x) = A_f E_f \varepsilon_f(x)$) and t_f is the CFRP thickness. From a global-level perspective, CFRP-debonding (that is, fracture of the interface) occurs if

$$G_{II}(x) \geq G_{IIcr} \quad (\text{II.13})$$

where G_{IIcr} is the critical energy release rate that may be obtained from the effective strain, ε_{fd} , at which debonding takes place (ACI 2017)

$$\varepsilon_{fd} = k \sqrt{\frac{f'_c}{nE_f t_f}} \leq 0.9\varepsilon_{fu} \quad (\text{II.14})$$

where n is the number of CFRP layers; k is a constant ($k = 0.083$ and 0.41 for psi and metric units, respectively); and ε_{fu} is the CFRP ultimate strain.

Implementation — The near-failure load of the beams was conservatively taken as 80% of their respective capacity before delamination of CFRP. As discussed above beside DIC pictures, such a load level complies with the strain compatibility requirement of the model. Figure 12.2(a) plots steel strains of the CG0 beam and the CGD series at the groove locations (the CG3 series showed similar responses). In all cases, the strains did not reach the yield strain of $\varepsilon_y = 0.0021$ in the investigation zone ($x \leq 250$ mm (10 in.), Figure 9). The behavior of the CFRP-termination region is considered elastic, except for the cracked concrete below the neutral axis of 50.9 mm (2.0 in.) to 55.4 mm (2.2 in.) from the top of the CGD beams. The predicted CFRP strains of the CG3 and CGD beams at each groove location are compared in Figure 12.2(b). These strains generally agreed with those measured in the laboratory, ranging from $\varepsilon_f = 0.0005$ to 0.0016 at $80\%P_u$ of the CGD beams (CGD-100 was typically shown in Figure 11.5(c)). Irrespective of strengthening configuration, the curvature-induced CFRP strains at Groove 1 were lower than others, corroborating the significance of the local interaction between the CFRP and the epoxy-filled groove on the interfacial failure in the vicinity of the CFRP-termination. The integrity of the interface at the groove locations is assessed in Figure 12.3(a). The energy release rates of the CG3-100 and CGD-100 beams

were higher than those of the CG3-0 and CGD-0 beams by 271% and 226%, on average, respectively. Nonetheless, the rates of all the beams were within the boundary of the critical value of $G_{IIcr} = 1.6 \text{ J/m}^2$ (0.11 lb/ft), which justifies the reason why interfacial damage at the groove locations was not observed in the laboratory.

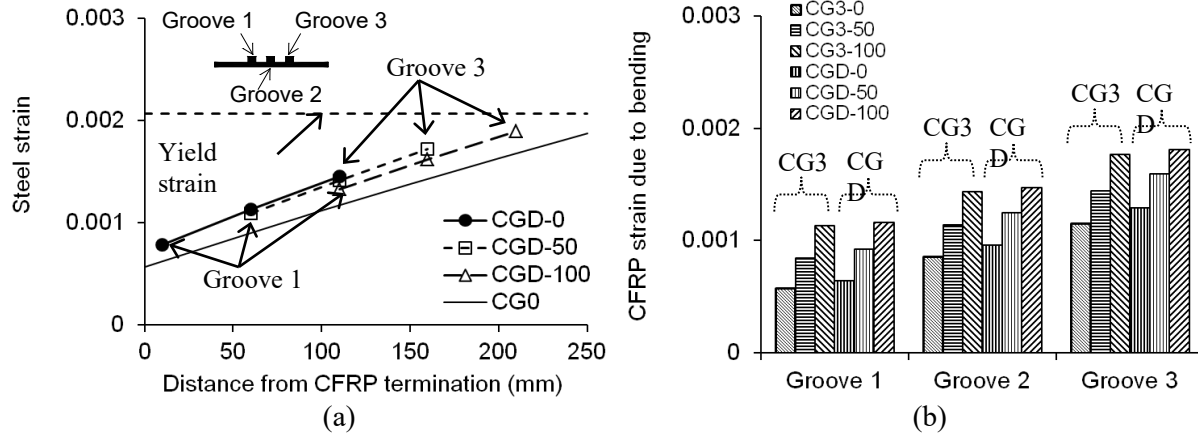


Figure 12.2 Development of steel and CFRP strains due to bending at near-failure of beams: (a) steel strain; (b) comparison at grooved locations

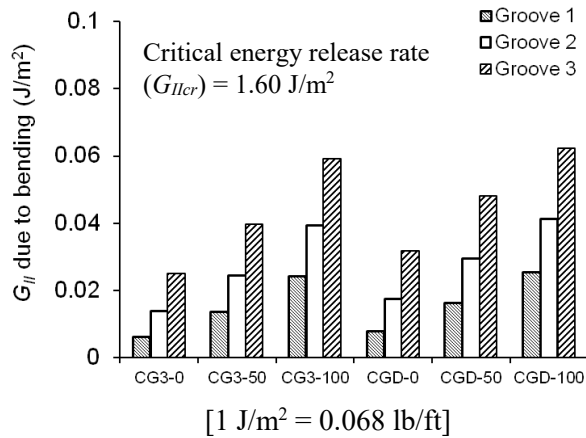


Figure 12.3 Assessment of integrity in CFRP-concrete interface

13. SUMMARY AND CONCLUSIONS

This paper has substantiated the potential of an alternative bonding scheme for strengthening concrete beams with CFRP sheets. Dissimilar to conventional CFRP-bonding, discrete grooves were cut and filled with an epoxy when CFRP sheets were placed to mitigate interfacial stresses, thereby impeding the onset of CFRP-delamination. Two types of groove arrangements were tested: three grooves near the CFRP-termination (the CG3 series) and distributed grooves along the beam span (the CGD series). The performance of these beams was comparatively assessed against that of the unstrengthened and plain CFRP-bonded beams, with an emphasis on load-carrying capacity, flexural responses, failure modes, and the progression of cracking and delamination. Analytical models were employed to clarify the interfacial behavior at the local and global levels. Implementation of the proposed bonding approach is practicable in the field, given that precut grooves are frequently used for installing near-surface-mounted (NSM) CFRP strips. A high-viscosity epoxy is suggested to avoid premature leaking until the bonding agent sets. The following conclusions were drawn:

- The load-carrying capacity of the beams with epoxy-filled grooves (CG3 and CGD) was higher than that of the unstrengthened (UNS) and plain CFRP-bonded (CG0) beams over 46%. The distance between the CFRP-termination and the nearest groove dominated the degree of the capacity enhancement, particularly for the beams with distributed grooves (CGD).
- The UNS beam exhibited typical flexural failure, accompanied by concrete cracking and crushing. The CG0 and CG3 beams failed by CFRP-delamination, which progressed gradually at the rebar level due to geometric discontinuities. The presence of the end grooves in the CG3 beams retarded stress transfer along the CFRP-concrete interface. Unlike these beams, the delamination was not observed in the CGD series that failed by shear cracking and concrete crushing. The distributed grooves restrained concrete deformation within the constant moment region and lessened the formation of flexural cracks.
- Owing to the pseudo-anchorage effect that constrained horizontal deformation of the interface layer, the grooved bonding schemes improved the pre-yield stiffness of the beams compared with the stiffness of the CG0 beam. The distributed grooves were effective in preserving the moment of inertia of the CGD beams and disrupting the sectional rotation at midspan.
- The steady development of CFRP strains in the CG0 beam became asymmetric as the beam was subjected to cracking and progressive delamination, which affected integrity of the strengthening system. The complex strain pattern of the CG3 beams illustrated irregular interaction between the local grooves and substrate concrete near the CFRP-termination. The tensile stresses of the CGD beams were distributed along the interface.
- The interface-level model showed that a groove at the CFRP-termination reduced the maximum stress by up to 78%, while the strength of the substrate concrete was not an influential factor in the range of $f'_c = 15 \text{ MPa}$ (2,200 psi) to 40 MPa (5,800 psi). Use of a low-modulus bonding agent reduced the development of the interfacial stress. The location of CFRP-termination was recommended to be close to the support. From a global-level standpoint, the energy release rate of the grooved interface was lower than the critical rate; hence, the fracture failure of the proposed bonding scheme was not noticed.

14. REFERENCES

- AASHTO. 2012. Guide specifications for design of bonded FRP systems for repair and strengthening of concrete bridge elements, American Association of State Highway Transportation Officials, Washington, D.C.
- ACI. 2007. Report on fiber-reinforced polymer (FRP) reinforcement for concrete structures (ACI 440R-07), American Concrete Institute, Farmington Hills, MI.
- ACI. 2014. Building code requirements for structural concrete and commentary (ACI318-14), American Concrete Institute, Farmington Hills, MI.
- ACI. 2017. Guide for the design and construction of externally bonded FRP systems for strengthening concrete structures (ACI 440.2R-17), American Concrete Institute, Farmington Hills, MI.
- Al-Sammari, A.T. and Brena, S.F. 2018. Finite element simulation and parametric study of anchored fiber-reinforced polymer sheets, *ACI Structural Journal*, 115(2), 365-377.
- ASTM. 2018. Standard test method for compressive strength of cylindrical concrete specimens (ASTM C39-18), American Society for Testing and Materials, West Conshohocken, PA.
- CSA. 2014. Canadian highway bridge design code (CSA S6-14), Canadian Standard Association, Toronto, On, Canada.
- CEB-FIP. 1993. CEB-FIP model code 1990, Thomas Telford, Lausanne, Switzerland.
- Ceroni, F., Pecce, M., Matthys, S., and Taerwe, L. 2008. Debonding strength and anchorage devices for reinforced elements strengthened with FRP sheets, *Composites Part B*, 39, 429-441.
- Colalillo, M.A. and Sheikh, S.A. 2014. Behavior of shear-critical reinforced concrete beams strengthened with fiber-reinforced polymer: analytical method, *ACI Structural Journal*, 111(6), 1385-1396.
- Eftkhar, M.R. and Ya'ghubi, M. 2016. Using boring to postpone debonding of CFRP-composite concrete beams, *Journal of Composites for Construction*, 20(1), 04015035
- El-Hacha, R., Wight, R. G., and Green, M. F. 2001. Prestressed fibre reinforced polymer laminates for strengthening structures.” *Progress in Structural Engineering and Materials*, 3, 111-121.
- El-Maaddawy, T. and Chekfeh, Y. 2012. Retrofitting of severely shear-damaged concrete T-beams using externally bonded composites and mechanical end anchorage, *Journal of Composites for Construction*, 16(6), 693-704.
- Garcia, J.E., Satrom, N.S., Jirsa, J.O., Ghannoum, W.M. 2018. Shear strengthening of concrete girders using carbon fiber-reinforced polymer sheets and anchors, *ACI Structural Journal*, 115(4), 1165-1173.
- Kalfat, R. and Al-Mahaidi, R. 2011. Investigation into bond behaviour of a new CFRP anchorage system for concrete utilising a mechanically strengthened substrate, *Composite Structures*, 92(11), 2738-2746.
- Khalifa, A., Alkhrdaji, T., Nanni, A., and Lansburg, S. 1999. Anchorage of surface mounted FRP reinforcement, *Concrete International*, 21(10), 49-54.

- Mostofinejad, D. and Mahmoudabadi, E. 2010. Grooving as alternative method of surface preparation to postpone debonding of FRP laminates in concrete beams, *Journal of Composites for Construction*, 14(6), 804-811.
- Pham, H. and Al-Mahaidi, R. 2004. Experimental investigation into flexural retrofitting of reinforced concrete bridge beams using FRP composites, *Composite Structures*, 66, 617-625.
- Smith, S.T. and Teng, J.G. 2001. Interfacial stresses in plated beams, *Engineering Structures*, 23, 857-871.
- Sui, L., Luo, M., Yu, K., Xing, F., Li, P., Zhou, Y., and Chen, C. 2018. Effect of engineered cementitious composite on the bond behavior between fiber-reinforced polymer and concrete, *Composite Structures*, 184, 775-788.
- Taljsten, B. 1997. Strengthening of beams by plate bonding, *Journal of Materials in Civil Engineering*, 9(4), 206-212.
- Wan, B., Sutton, M.A., Petrou, M.F., Harries, K.A., and Li, N. 2004. Investigation of bond between fiber reinforced polymer and concrete undergoing global mixed mode I/II loading, *Journal of Engineering Mechanics*, 130(12), 1467-1475.